Kinematic analysis of brittle roto-translational planar and listric faults based on various rotational to translational velocities of the faulted blocks

Submitted to

Indian Institute of Science Education and Research Pune In Partial Fulfillment of the requirement for the BS-MS Degree Programme

By

Lokesh Tayade

Reg No. 20141123

IISER PUNE

Indian Institute of Science Education and Research Pune

Supervisor: Prof. Shyam S. Rai

Professor and Chair, Earth and Climate Science (IISER Pune)

Cosupervisor: Prof. Soumyajit Mukherjee

Department of Earth Sciences (India Institute of Technology Bombay)

CERTIFICATE

This is to certify that this dissertation entitled **Kinematic analysis of brittle roto-translational planar and listric faults based on various rotational to translational velocities of the faulted blocks** towards the partial fulfilment of the BSMS dual degree programme at the Indian Institute of Science Education and Research, Pune represents study/work carried out by **Lokesh Tayade** at IISER Pune and IIT Bombay under the supervision of Supervisor: **Prof. Shyam S. Rai**, Professor and Chair Earth and Climate Science (IISER Pune), **Prof. Soumyajit Mukherjee**, Department of Earth Sciences (Indian Institute of Technology Bombay), during the academic year 2018 – 2019.

Lokesh Tayade

Prof. Shyam S. Rai

Committee:

Name of Guide: **Prof. Shyam S. Rai**

Name of TAC: **Prof. Shreyas Managave**

DECLARATION

I hereby declare that the research work presented in the report entitled **Kinematic analysis of brittle roto-translational planar and listric faults based on various rotational to translational velocities of the faulted blocks** have been carried out by me at the Department of Earth and Climate Science (IISER Pune), Department of Earth Sciences, Indian Institute of Technology Bombay under the supervision of Prof. Shyam S. Rai and co-supervision of Prof. Soumyajit Mukherjee and the same has not been submitted elsewhere for any other degree.

Prof. Shyam S. Rai

Lokesh Tayade

Acknowledgments

I am very thankful of my thesis advisors **Prof. Shyam S. Rai** (Professor and Chair; Dept Earth and Climate Science, IISER Pune) **and Prof. Soumyajit Mukherjee** (Department of Earth Sciences, Indian Institute of Technology Bombay). Prof. Soumyajit Mukherjee was always encouraging and kept me motivated. He helped me whenever I ran into trouble or had a question about my research or writing. I would also like to thank the experts **Prof. Shreyas Managave** (Dept Earth and Climate Science, IISER Pune) who was my thesis advisor. I would like to thank **IISER Pune** for giving this opportunity.

Finally, I express my gratitude to my **parents** and my **friends** and my **roommate** for providing me with constant support and continuous encouragement throughout my years of study and through the process of researching and writing this thesis. This accomplishment would not have been possible without them. Thank you.

Contents

List of Figures

List of Tables

Abstract

This work models slickenside lineation patterns on planar and listric fault planes for different ratios of rates of rotation to the linear velocity or uniform speed towards a specific geographic direction ("ω/v") of the faulted blocks. These curves for the planar fault plane cases are fitted with natural examples of such roto-translational faults. In our ten chosen examples, the "ω/v" ratio ranges 0.2 (fault at San Miguelito range, Central México) to 2.4 (fault at Hyogoken-Nambu, Japan). Knowing the most reasonable "ω/v" ratios from terrains can better interpret its tectonics. As several hydrocarbon reserves are related to roto-translational faults, this work will presumably have a far-reaching implication in petroleum geosciences.

Introduction

Deciphering kinematics of faulting is one of the fundamental exercises in structural geology (e.g., Rowland and Sibson 2001). Having diverse geometries, slickensides may develop on fault planes indicate either 180° apart two possible directions or a unique direction of slip (Doblas et al. 1997, Doblas 1998; Mukherjee 2014, 2015; Dasgupta and Mukherjee 2017).

In nature, purely translational faults (Fig. 1a) with perfectly straight slickensides are found rarely. A true rotational fault (Fig. 1b1) has neither yet been reported in geoscience literature. Natural slickensides, on the other hand, are usually gently to moderately curved indicating that the faulted blocks rotate to some amount when they translate (review in Mukherjee and Khonsari 2017). Such lineations indicate neither a first translation followed by rotation nor a vice versa, as in those cases two distinct lineation patterns would have developed- one perfectly linear and another flawlessly circular. Only in cases of ideal dip slip and strike slip book-shelf gliding (Mukherjee 2018; Mukherjee and Khonsari 2018), significantly rotated crustal blocks can leave straight slickensides at the fault surface, i.e., at the interfaces between the two books/crustal blocks. Mandal and Chakraborty (1998) refer the natural faults with simultaneous rotation and translation as the roto-translational faults (Fig. 1c).

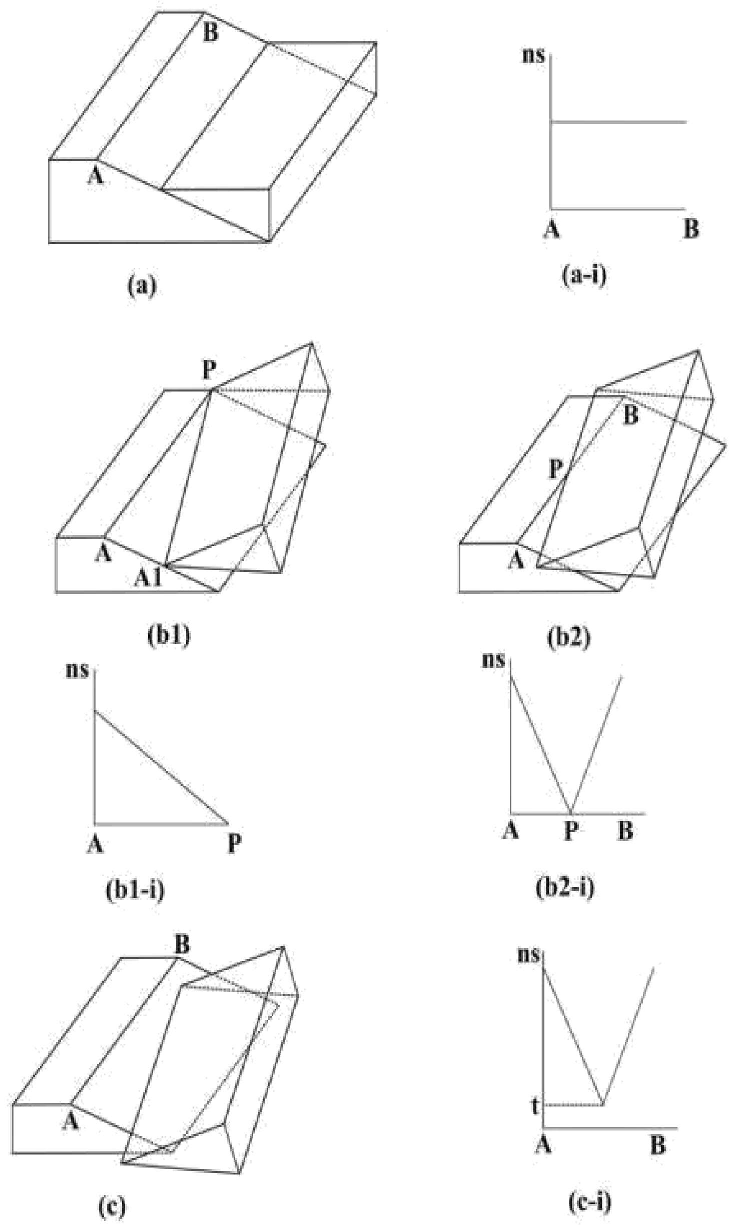

Fig. 1. Ideal faults. **a.** Translational normal fault. **a-i.** Net-slip is constant. **b1-b2.** Pure rotational fault. **b1-i**. Net-slip is zero at P and highest at A. **b2-i**. Net-slip is zero at p and highest at A and B. **c.** Roto-translational fault. **c-i.** Its net-slip profile. Reproduced from fig. 1 of Mukherjee and Khonsari (2017).

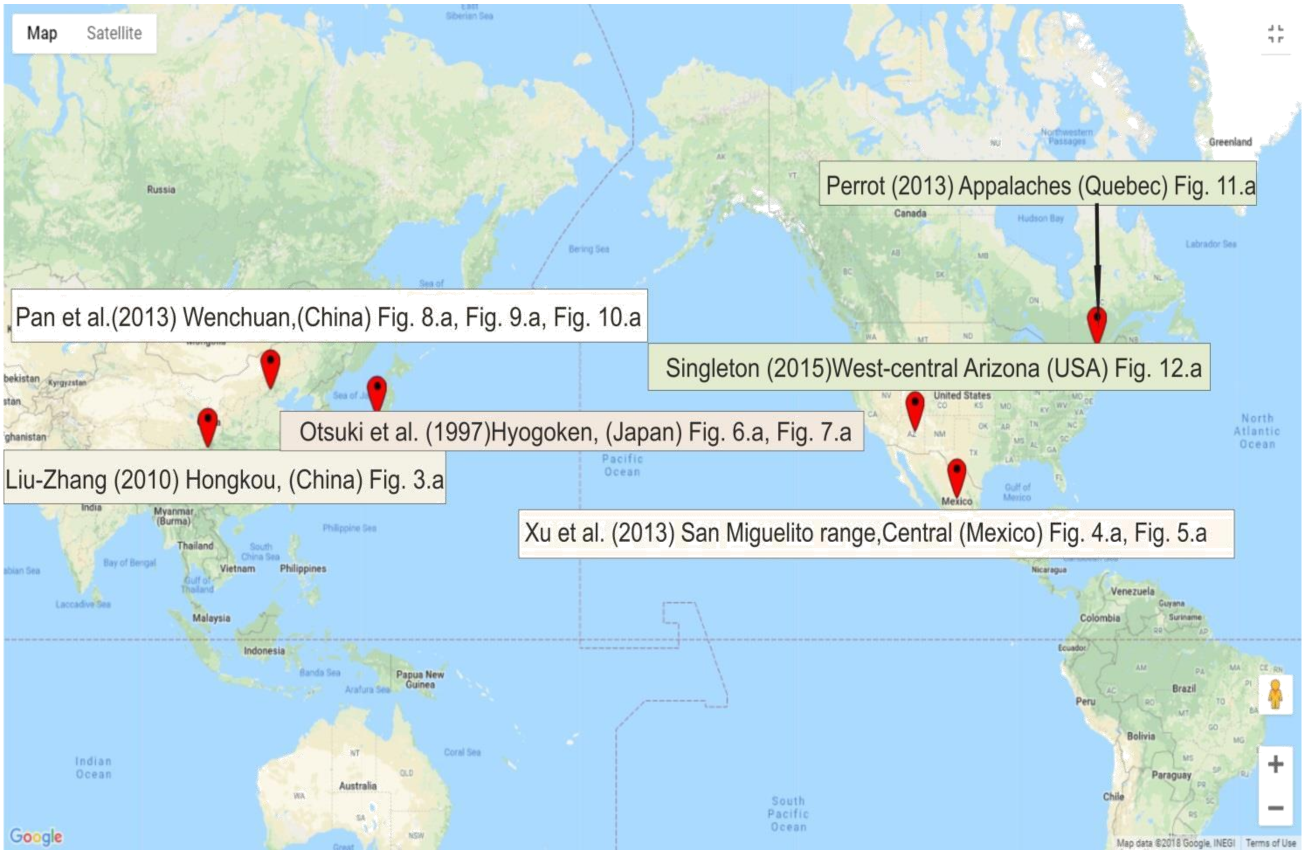

Fig. 2: Global distributions of fault with curved slickensides photographed

Fig. 2 presents the global distribution of such faults where curved slickensides have been photographed by the previous authors. Robert Twiss published several papers on theoretical analyses of rotational fault kinematics based on tangent lineation diagrams using curved slickensides (e.g., Twiss et al. 1991). Roto-translational faults can be planar or listric (referred in Ghosh, 1993; Marshak and Mitra, 1988) and can be numerous in specific terrains (Nevin, 1949). Listric faults, on the other hand, have classically been presented implicitly in structural geology text mostly to be dip-slip normal faults (e.g., Fossen 2016; Blue Mountain Fault, Australia: Mackenzie (1993); numerical models: Hjelle 2014). However, strike-slip and oblique-slip listric faults have also been reported cursorily in the literature.

I. strike-slip listric faults have been reported in mega-scale from both the continental and oceanic crusts: at the releasing bend at the Loreto basin (Dorsey et al. 1995), ridge basin, southern California (May et al. 1993), Loma Prieta bend in the San Andreas Fault (Tearpock and Bischke 2002), the pull-apart Bhima basin (south India) (Dey 2015), the boundary between Eurasian continental crust and Pacific oceanic crust (TPED, CPC 1992), the Brevard fault zone (southern Appalachians) (Vouchez 1987), to name a few. Flower structures and transpressive basins consist of strike-slip listric fault planes. Rodgers and Chinnery (1969) describe strain and displacement patterns for strike-slip faults but do not simulate stretching lineation geometries on them.

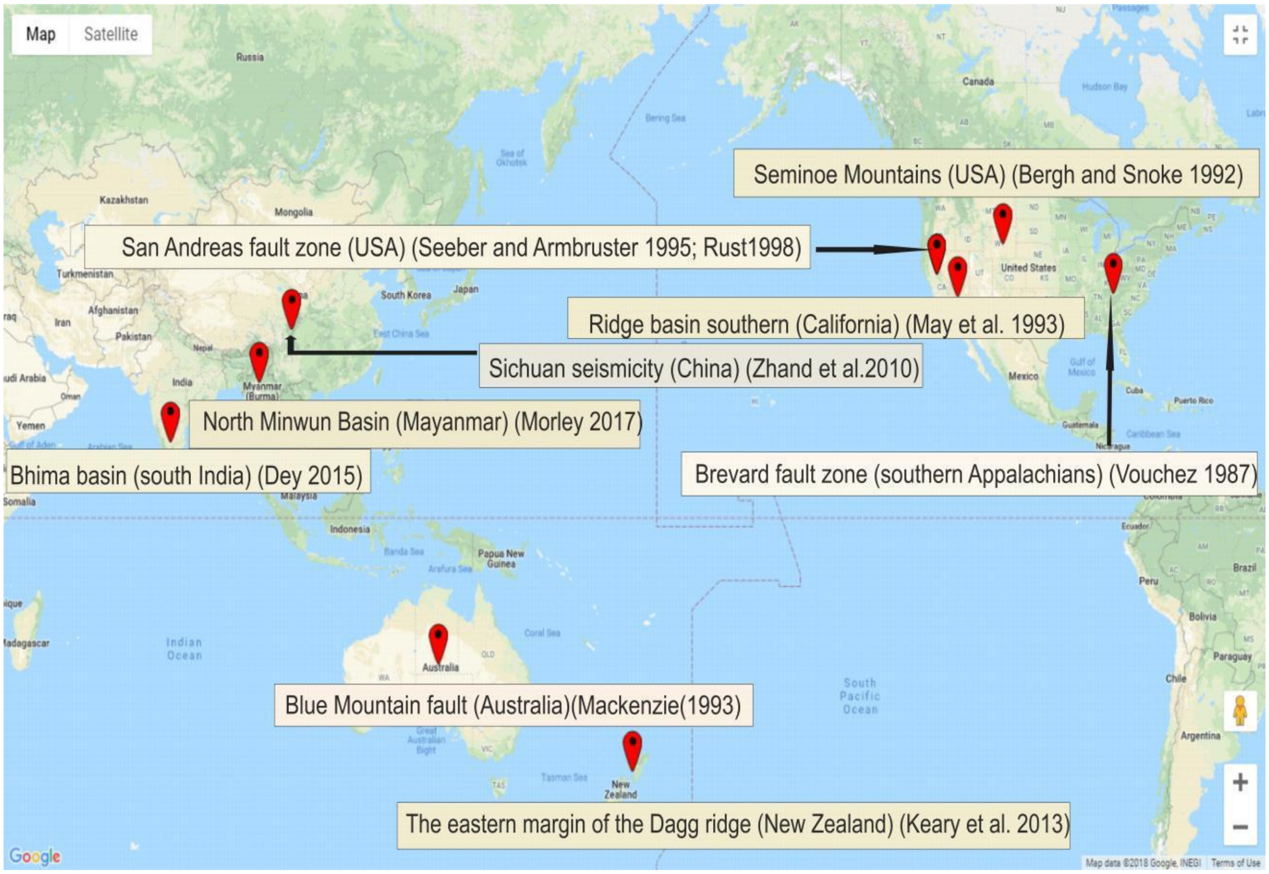

Fig. 3. Global locations of reported oblique slip listric faults.

II. Oblique-slip listric faults (Fig. 3) have been briefly reported from the North Minwun Basin (Myanmar) (Morley 2017), the eastern margin of the Dagg ridge (New Zealand) (Keary et al. 2013). Seminole Mountains (U.S.) (Bergh and Snoke1992), the San Andreas fault zone (Seeber and Armbruster 1995; Rust 1998), syn-sedimentary slide from the Waitemata basin (New Zealand) (Sporli and Rowland 2007), half-graben structures (Jayko and Bursik 2011), the 12-May-2008 Sichuan seismicity in China (Zhand et al. 2010), the pop-up structures (Nabavi et al. 2017) etc. Unlike these authors, Claypool et al. (2002) describe a palm tree-like network of oblique-slip listric faults from Fiordland (New Zealand). Besides merely reported (Ghosh, 1993; Marshak and Mitra, 1988), quantification of curvature of listric faults does not exist in the structural geological and the tectonic literature till date. Davis et al. (2019) discuss recently the kinematics of listric faults in 3D. While they describe how shear fractures are associated with such faults, the lineation pattern developed on the listric faults has not been explained.

This Thesis has two parts.

I. Kinematic analysis of roto-translational faults with planar and curviplanar/listric fault surfaces: The loci of slickenside developed on such fault planes are modeled, and then correlated with field-photos. II. For different ratios of "ω:v", geometries of slickensides on curved fault planes are simulated. Since curved lineations on curved fault planes have merely been reported, but the previous authors did not provide any image, the simulated curves in ideal cases remain uncorrelated with the natural examples. Several hydrocarbon reserves are associated with roto-translational faults (e.g., Afifi et al.,2016). The present study in the long run can be therefore useful in petroleum geoscience.

2. *Curved slickensides and fault block rotation (rates)*

Twiss and Gefell (1990) describe the basic kinematics of curved slickenfibres. However, they do not work out the rotation rate with respect to the translational velocity. Kusky et al. (1997) report up to 55° of curvature of the lineation on fault plane. A review of the literature indicates that coseismic faulting can produce curved slickenlines (e.g., fig. 12 in Liu-Zeng et al. 2010), but exceptions do exist (fig. 6b in Pan et al. 2014). Otsubo et al. (2013) report the most strikingly curved slickenside on the fault plane related to the 11-April-2011 Mw = 6.8 earthquake from the Iwaki city (Japan). On the other hand, Pan et al. (2014) report a gently curved co-seismic striation on fault planes (their fig. 6b) as a result of 12-May-2008 Mw = 7.9 seismicity in Wenchuan (China). Slip rates for translational faults of various types have been deduced geochronologically, which usually range from a few mm- (Dezes et al., 1999) up to a few cms per year (Kohn et al., 2004). Mukherjee and Khonsari‟s (2018) literature survey in their table 1 reports a maximum rotation rate of crustal block 40° Ma^{-1} from North Iceland volcanic rift zone. Paleomagnetic studies have revealed considerable rotation and rotation rates from several terrains (review in Table1). However, from these places, curved slickensides have not been reported. Price and Scott (1994) provide a much-reduced rate of rotation of 3 ° Ma^{-1} from SW Turkey. Horst et al. (2018) recently reported a pronounced rotation of the crustal block up to 105° from the Húsavík-Flatey Fault (Iceland).

Table 1. Rotational information from different terrains in the world.

Author(s)	**Locations**	**Rotation rate (^{0} Ma^{1})**	**Total rotation (in ^{0})**
Pueyo et al. (2002)	Thrust system in the External Sierras (Southern Pyrenees)	5.3 to 21	At leat 40
Mochale et al. (2012)	Thrust belt around Boltana anticline, southern Pyrenees	1 to 10	52
Rodriguez-Pinto et al. (2016)	Around Balzes anticline (Southern Pyrenees)	5.2	No data
Oliva-Urcia and Pueyo (2007) and ref.therein	West of South Pyrenean Central Unit	No data	25 to 50
Oliva-Urcia and Pueyo (2007) and ref.therein	Eastern part of South Pyrenean Central unit	No data	80
Oliva-Urcia and Pueyo (2007) and ref.therein	Internal Sierras, southwest Pyrenees	No data	08 to 26

Model

The geometries of curved slickensides developed at different ratios of angular (ω) to linear velocities (v) of the faulted blocks are modeled using the programming software RStudio (Version1.0.153-2009-20017). While the angular velocity represents the rotational component of faulting, the linear velocity denotes that for the translational component of movement between the two faulted blocks. The modeled curves generated were then fitted with already published ten good quality field photographs of planar fault planes with prominent curved (non-circular) slickensides (Table 2), using the Rhinoceros curve-fitting software (version 6 SR9 6.9.18271.20591). By finding the best fit, the "ω:v" ratios are deduced in each case. In some cases the slickensides appear to have developed on gently curvilinear surfaces, such as fig.3 of Tapsoba and Howard (2017), thus restricts the use of every example of curved lineations from already published figures.

Lineation‟s that have developed on planar fault surfaces are analyzed in the first part of this work. In three simple tests, the model is found to match the common sense. To cross-check whether the RStudio-derived graphs(Code in Appendix 1) gave realistic results, first, when $\omega/v = 0$, i.e., $\omega = 0$ and $v \neq 0$, a linear slickenside is simulated (Fig. 4a).

Table 2. Numerical details of curve fitting exercise.

SI. No.	Previous workers	Previous workers' fig. No.	Location	ω/v Specified after curves were fitted	Fig. No. In this article	The correlation coefficient (the R-values)
1	Liu-Zang (2010)	12	Hongkou (China)	0.6	Fig. 8a	0.96
2	Xu et al (2013)	4a	San Miguelito (Mexico)	0.4	Fig. 9a	0.95
3	Xu et al. (2013)	4c	San Miguelito (Mexico)	0.2	Fig. 10a	0.95
4	Otsuki et al. (1997)	6a	Hyogoken (Japan)	1.4	Fig. 11a	0.95
5	Otsuki et al. (1997)	6b	Hygoken (Japan)	2.4	Fig. 12a	0.95
6	Pan et al. (2013)	7c	Wenchuan (China)	0.6	Fig. 13a	0.96
7	Pan et al. (2013)	8d	Wenchuan (China)	0.4	Fig. 14a	0.96
8	Pan et al. (2013)	11c	Wenchuan (China)	0.2	Fig. 15a	0.95
9	Perrot (2013)	2.4 a	Appalaches (Quebec)	1.6	Fig. 16a	0.95
10	Singleton (2015)	4a	Metamorphic core complex,west-central Arizona(USA	0.6	Fig. 17a	0.96

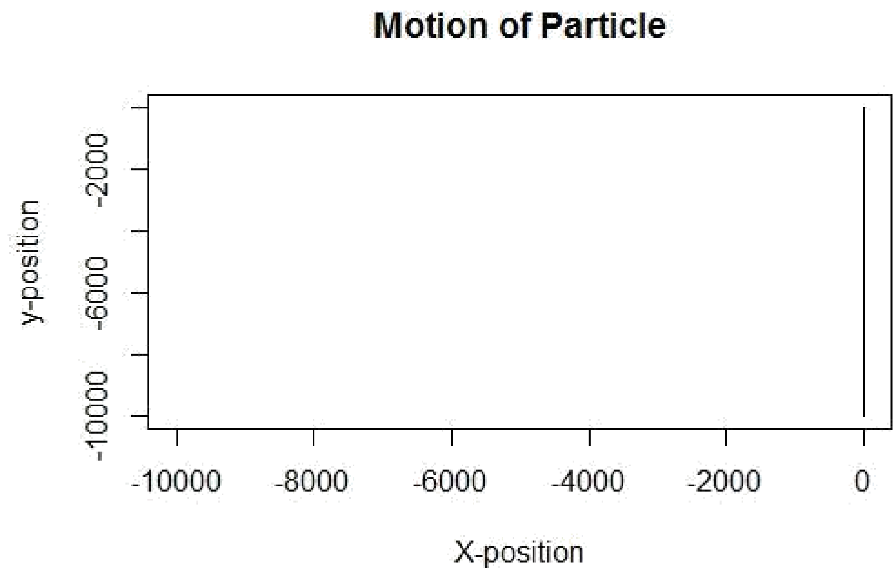

Fig. 4a. The modeled lineation geometries on a planar fault plane ω = 0 cases.

This is the case of a purely translational fault (Fig. 1a). Second, when ω/v is "undefined", i.e., v = 0 (such as Fig. 1b1), the slickenside appears as merely a point

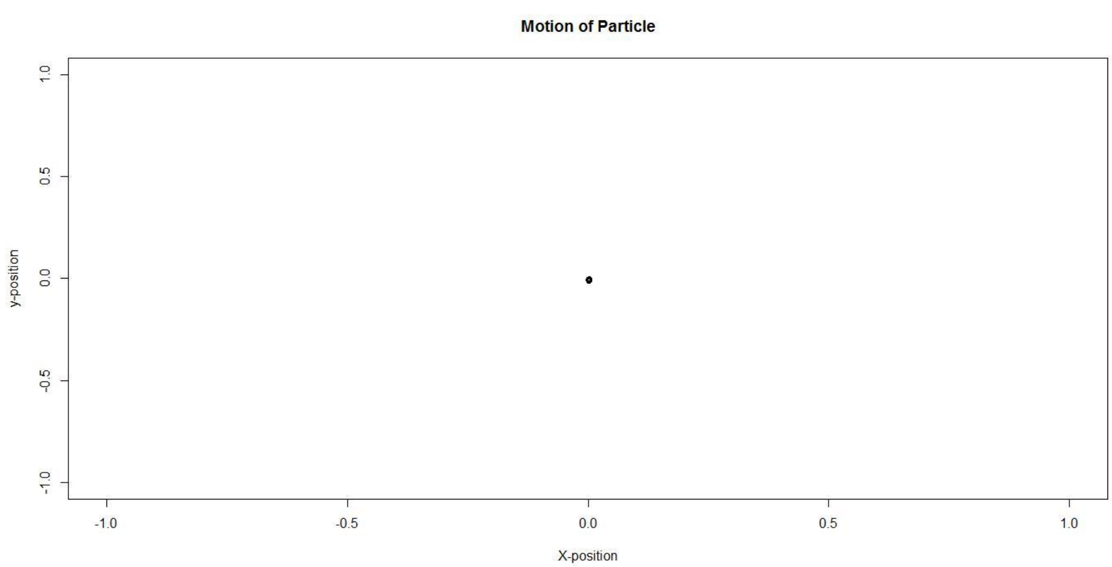

Fig. 4b. The modeled lineation geometries on planar fault planes v = 0 case.

Since v = 0, the point does not translate to attain a linear geometry; rather it only rotates about itself. Third, the higher the ω/v magnitude, more curved is the slickenside. For example, compare the curve in Fig. 4.c1 which is having less curvature than that in Fig. 4.c2, where ω/v are 1.3 and 5.6, respectively.

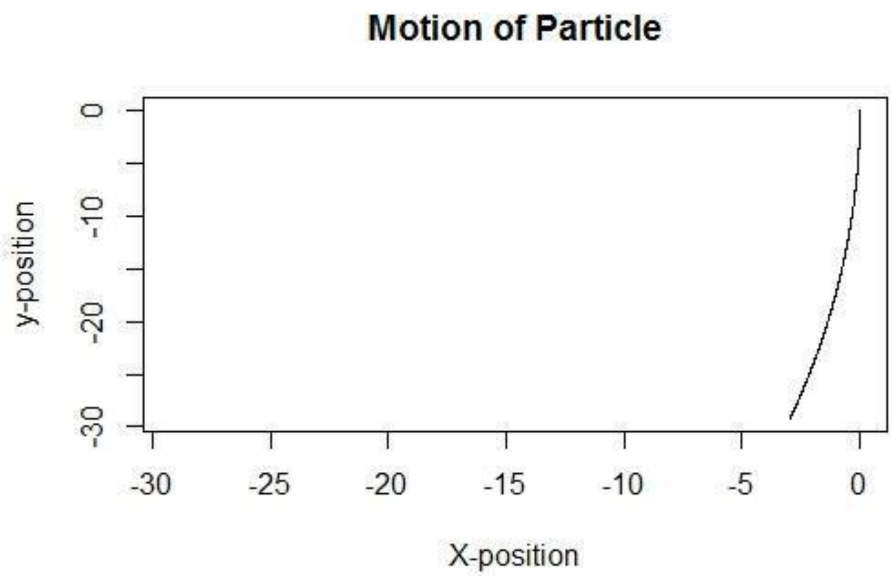

Fig. 4c1. The modeled lineation geometries on planar fault planes $\omega \neq 0$, $v \neq 0$ case (here $\omega/v = 1.3$).

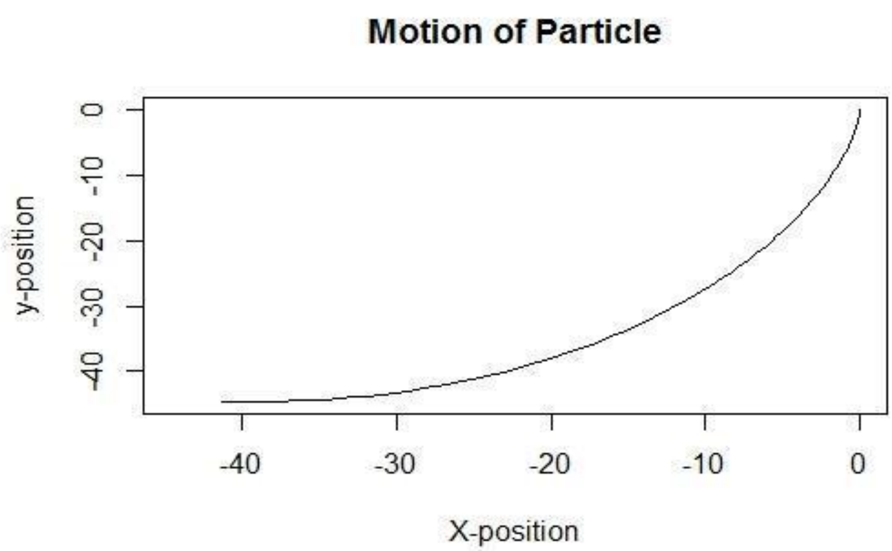

Fig. 4c2. the modeled lineation geometries on planar fault planes $\omega \neq 0$, $v \neq 0$ case (here $\omega/v = 5.6$).

The lineation geometries simulated in work remain the same for normal, reverse and strike-slip movement of the translational component of faulting.

The model curves produced by RStudio (sub-figures c in Fig. 8 to Fig.17). The Rhinoceros curve-fitting software was used to find the correlation coefficient (R) between the traces of lineations (sub-figures d in Fig. 8 to Fig.17 and the results viz., the “ω/v” ratio and the R values are presented against the corresponding slickensides in Table 1.

In the second part of this work, the software Matlab (Version 9.3, 2017) was used to simulate the geometry of the lineations in 3D developed on listric fault planes that are perfectly spherical(Appendix -2) Fig. 5 presents such a lineation pattern when the hanging wall block moves with respect to the footwall block along a specific geographic direction with a constant speed (also represented by “v” in this work so that one can compare this with the previous case of “constant velocity”). Since the faulted block slides past along a curved surface, using the term “constant velocity” would be inappropriate.

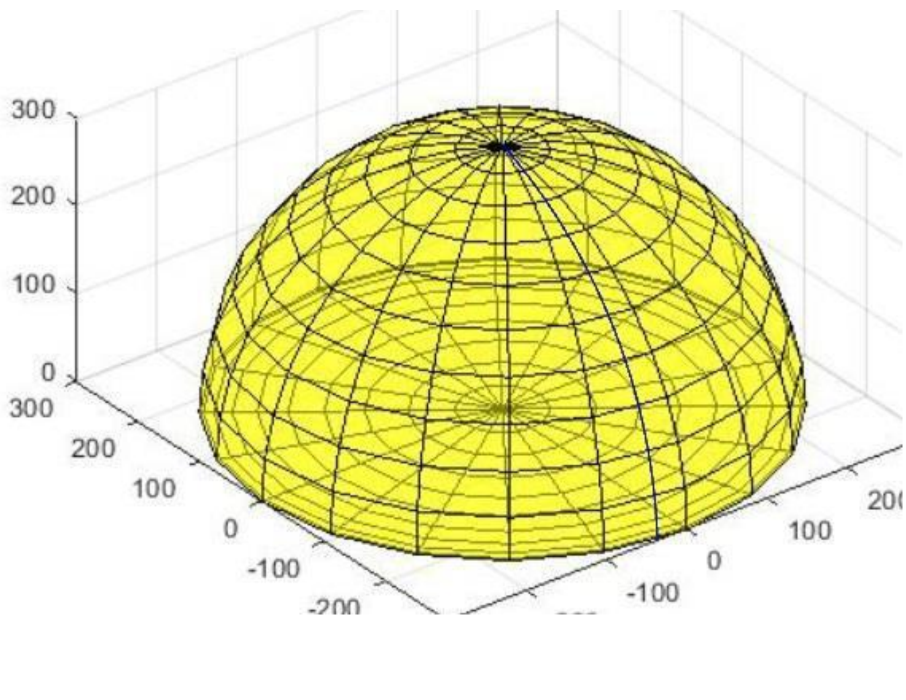

Fig. 5. Curved slickenside on the part of a spherical surface with radius = 200 units. ω = 1 unit per unit time.

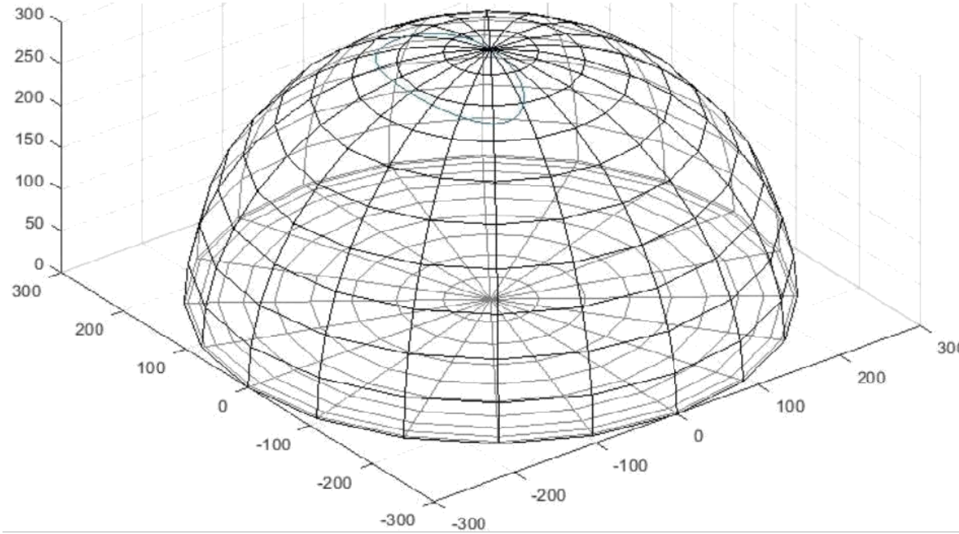

Fig. 6. Curved slickenside (blue-colored) with perfect rotational motion on the part of a spherical surface with radius = 200 units. The radius of sphere 300 unit, ω = 3 units per unit time.

Fig. 4b would simulate the lineation geometry if the spherical surface were converted to a planar surface.

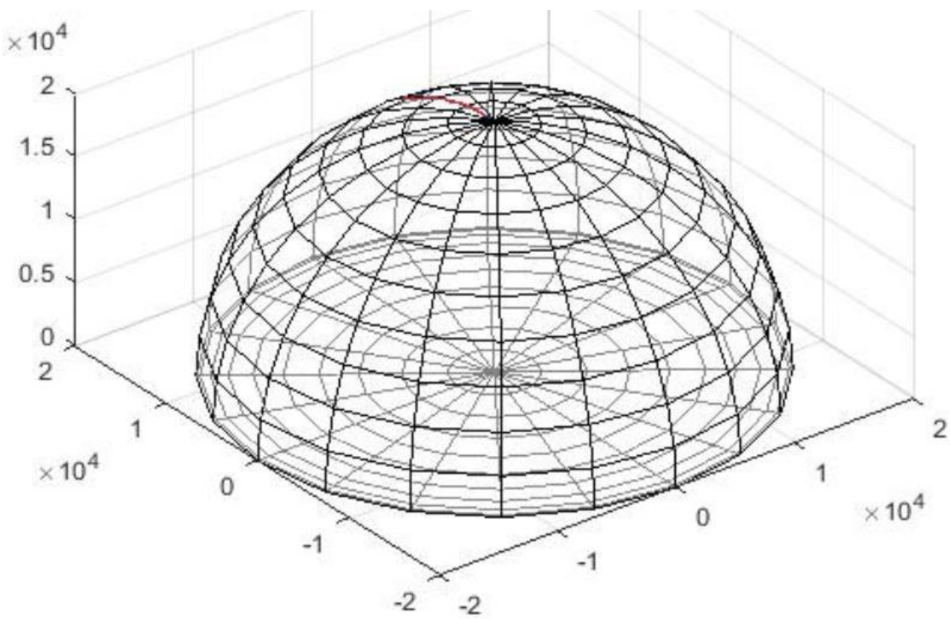

Fig. 7. purpose of this figure is to demonstrate the lineation geometry when ω = 0 on the part of a spherical surface with radius = 20000 units.

Radius chosen in this case is much more than that in Fig. 6 To observe the curved lineation at a higher resolution. Here the lineation generated is red-colored. Fig. 7 represents the lineation geometry when ω = 0. Note the lineation, in this case, is a segment of a circle, as expected. Figs. 18 to 28 are the several cases of lineations produced by different "ω/v" magnitudes. As no published photographs of lineations exist on spherical listric fault planes till date to our knowledge, correlating them with the natural examples is indeterminate.

THE CURVE FITTING EXERCISE

Subfigure „a" from Fig. 8 to Fig. 17 represents the Natural lineations on the fault plane from various authors. Subfigure „b" from Fig. 8 to Fig. 17 represents the traces of lineations (black colored line) traced back by me. Subfigure „c" from Fig. 8 to Fig. 17 represents the modeled lineation, and subfigure" from Fig. 8 to Fig. 17 represents the fit between curves in the sub-figure b and the sub-figure c. In all the subfigures" from Fig. 8 to Fig. 17 black curve is of natural lineation, and yellow curve is modeled curve which is plotted in Rhinoceros software (version 6 SR9 6.9.18271.20591).

Fig. 8a. Natural lineations on fault planes (from fig. 12 in Liu-Zang (2012)).

Fig. 8b. Traces of lineations (traced by me).

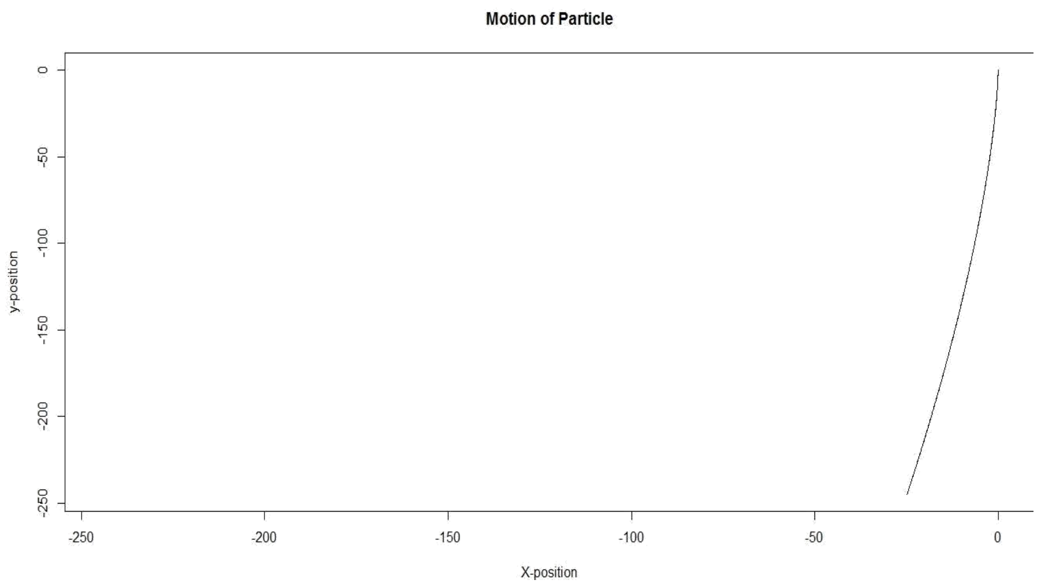

Fig. 8c. The modeled lineation for specific magnitudes of “ω/v” ratio, obtained by using The RStudio(Version1.0.153-2009-20017).

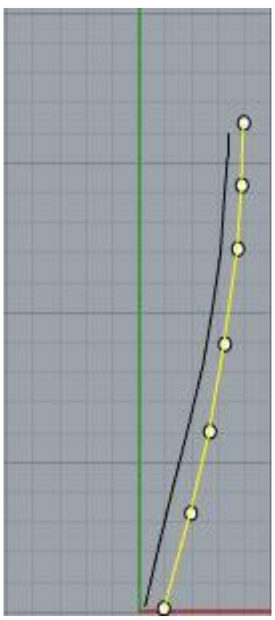

Fig. 8d. Fit between curves in the sub-figure b and the sub-figure c, black curve is natural lineation, and yellow curve is a model curve.

Fig. 9a. Natural lineations on fault planes (from fig. 4a from Xu et al. (2013)).

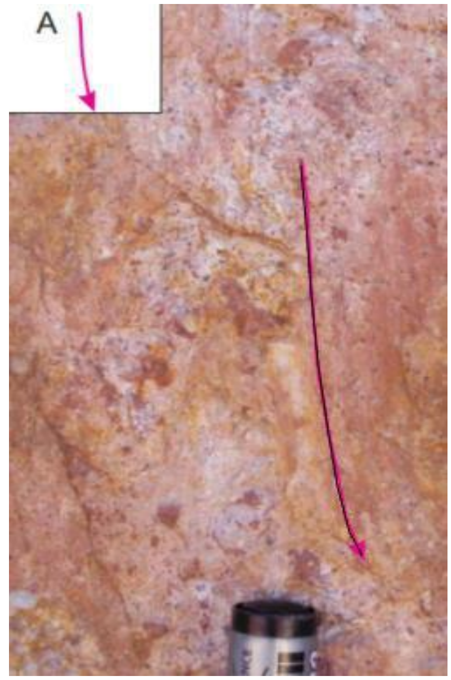

Fig. 9b. Traces of lineations black curve (traced by me).

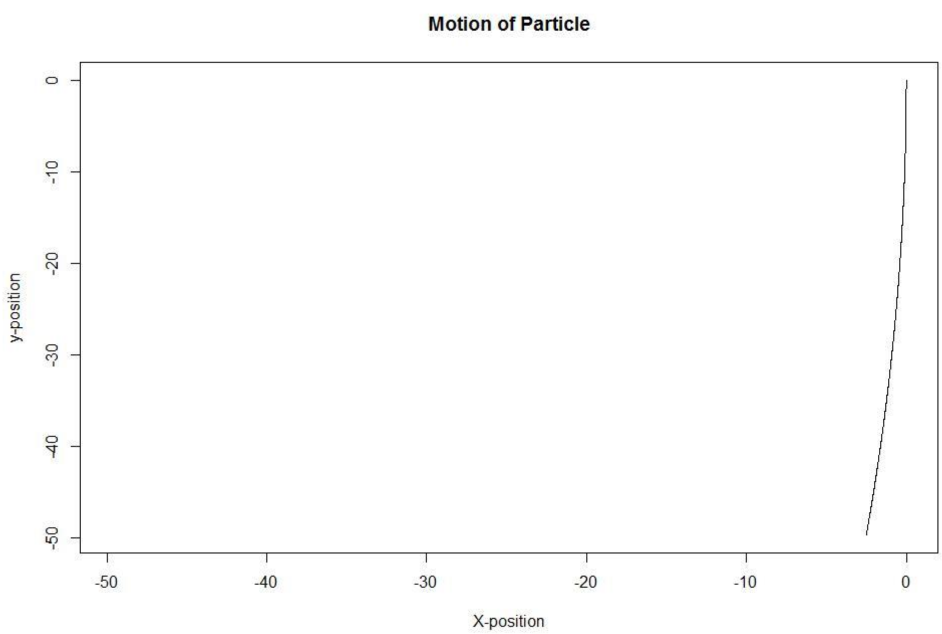

Fig. 9c. The modeled lineation for specific magnitudes of “ω/v” ratio, obtained by using The RStudio (Version1.0.153-2009-20017).

Fig. 9d. Fit between curves in the sub-figure b and the sub-figure c, black curve is natural lineation, and yellow curve is a model curve.

Fig.10a. Natural lineations on fault planes. (from fig. 4c in Xu et al (2013)).

Fig.10b. Traces of lineations black curve(traced by me).

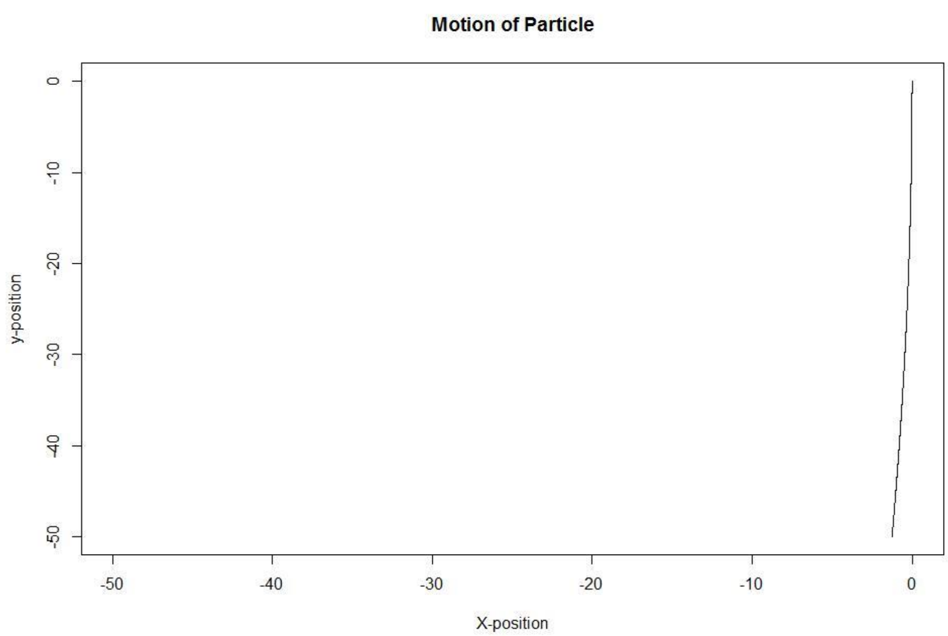

Fig. 10c. The modeled lineation for specific magnitudes of "ω/v" ratio, obtained by using The RStudio (Version1.0.153-2009-20017).

Fig. 10d. Fit between curves in the sub-figure b and the sub-figure c, black curve is natural lineation, and yellow curve is a model curve.

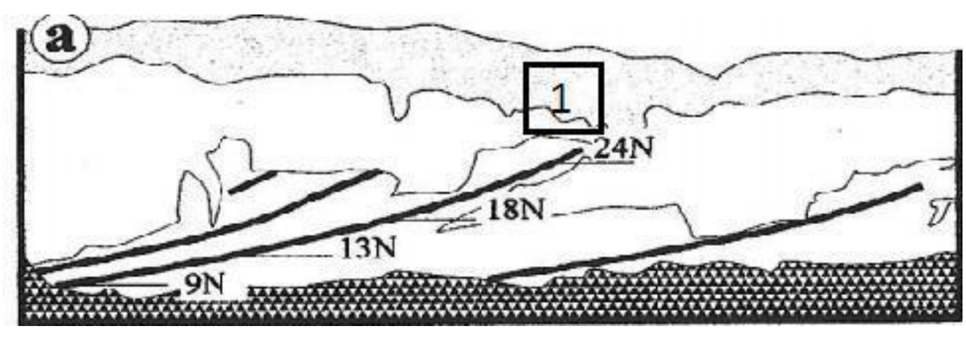

Fig. 11a. Natural lineations on fault planes (from fig. 7c in Otsuki et al. (1997)).

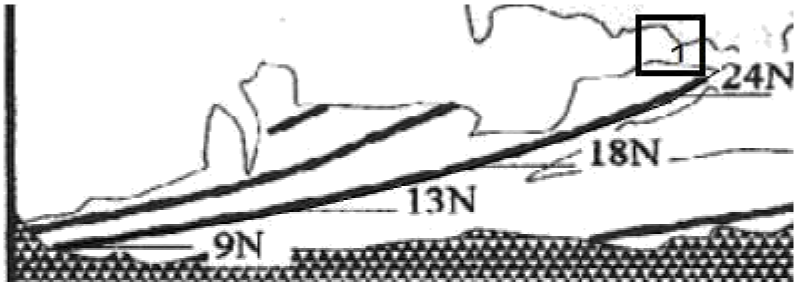

Fig. 11b. Traces of lineations (traced by me).

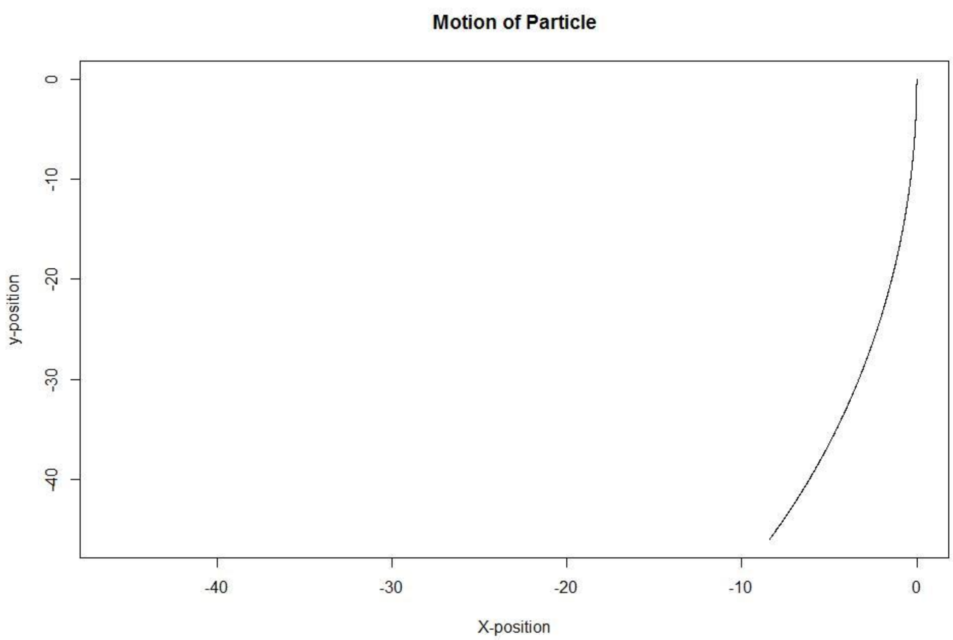

Fig. 11c. The modeled lineation for specific magnitudes of “ω/v” ratio, obtained by using The RStudio (Version1.0.153-2009-20017).

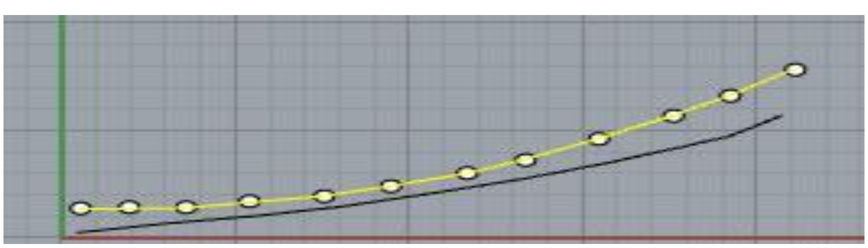

Fig. 11d. Fit between curves in the sub-figure b and the sub-figure c, black curve is natural lineation, and yellow curve is a model curve.

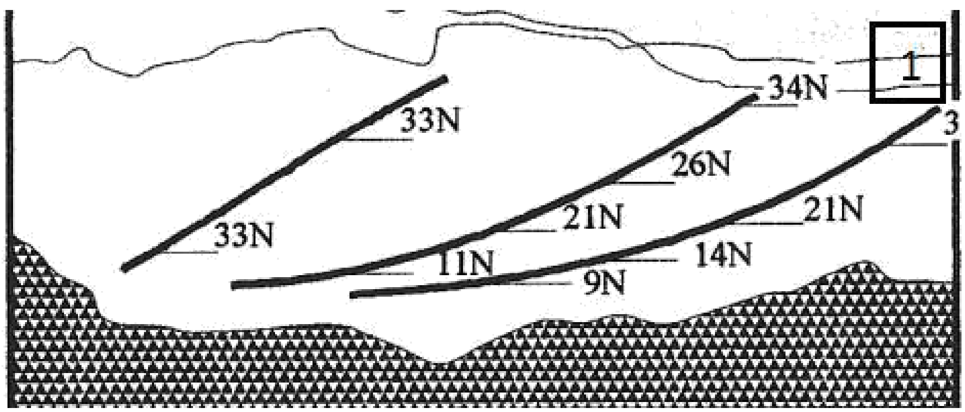

Fig. 12a. Natural lineations on fault (from fig. 8d in Otsuki et al. (1997))

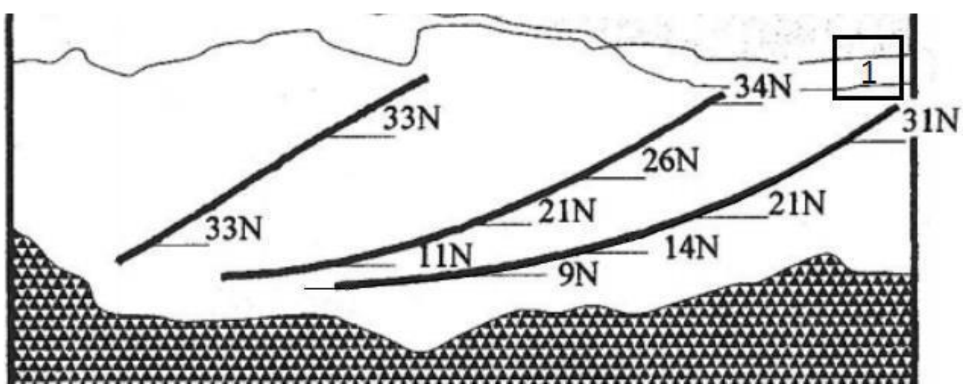

Fig. 12b. Traces of lineations (traced by me).

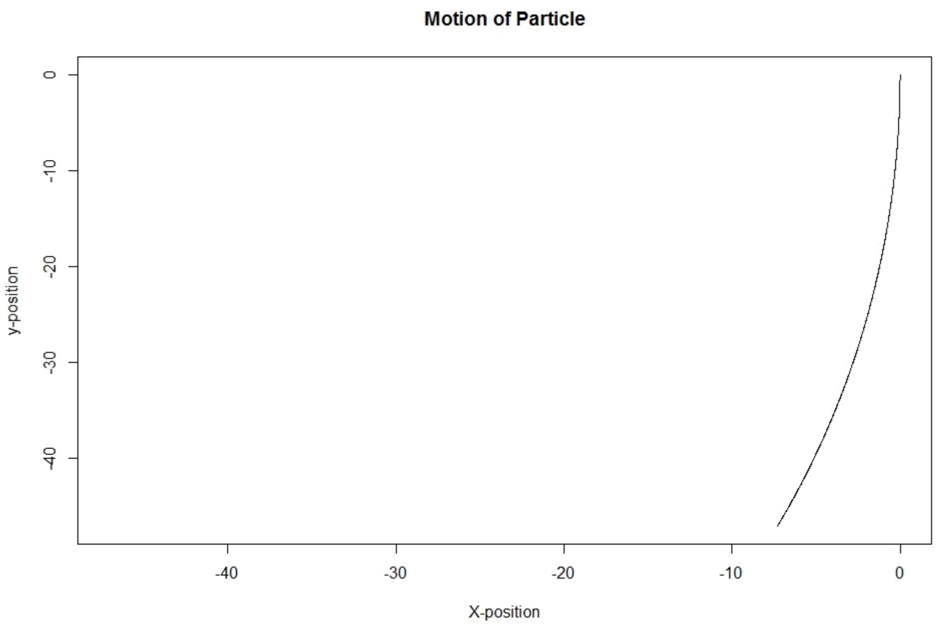

Fig. 12c. The modeled lineation for specific magnitudes of “ω/v” ratio, obtained by using The RStudio (Version1.0.153-2009-20017).

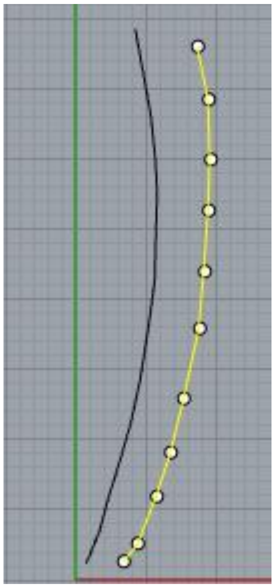

Fig. 12d. Fit between curves in the sub-figure b and the sub-figure c, black curve is natural lineation, and yellow curve is a model curve.

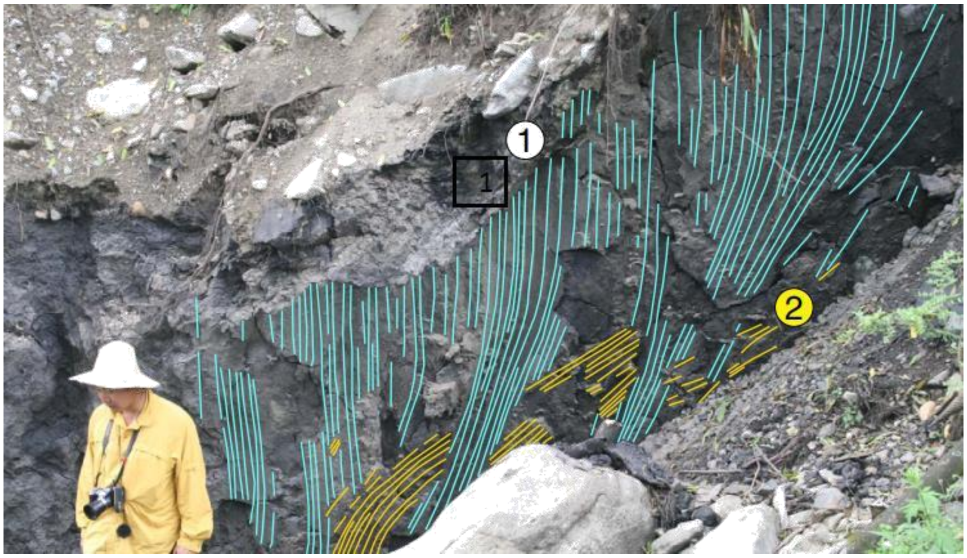

Fig. 13a. Natural lineations on fault planes (from fig. 7c in Pan et al. (2013)), blue and yellow two types of lineations are seen only blue ones are considered in this work.

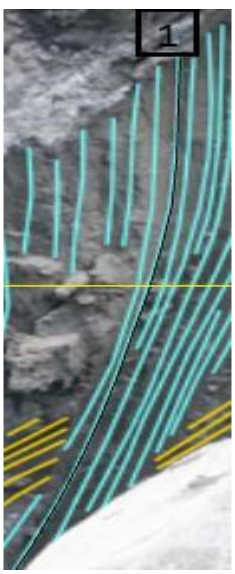

Fig. 13b. Traceback of lineation black curve (traced by me).

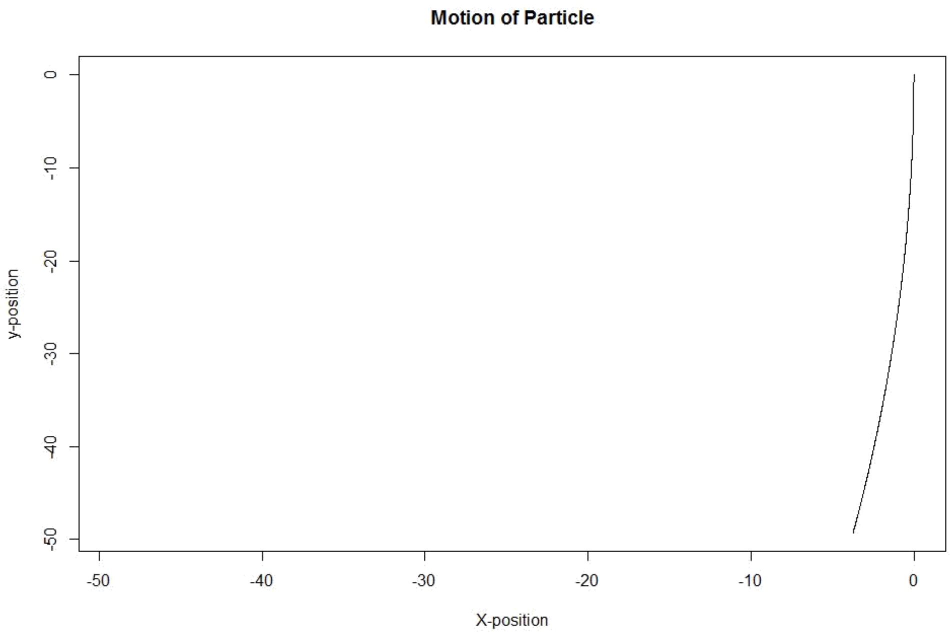

Fig. 13c. The modeled lineation for specific magnitudes of “ω/v” ratio, obtained by using the The RStudio (Version1.0.153-2009-20017).

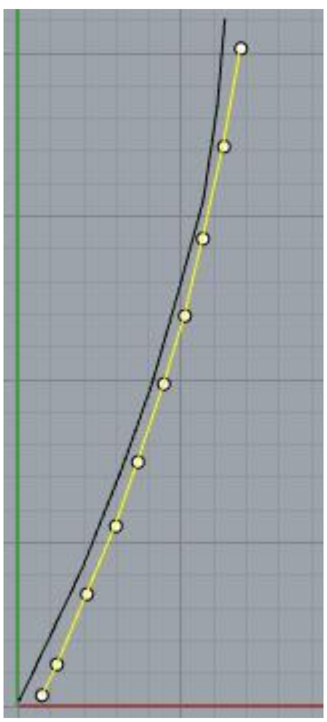

Fig. 13d. Fit between curves in the sub-figure b and the sub-figure c, black curve is natural lineation, and yellow curve is a model curve.

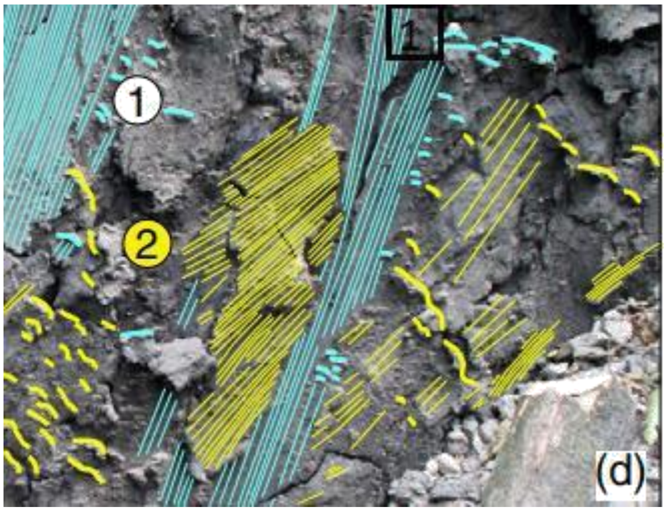

Fig. 14a. Natural lineations on fault planes (from fig. 8d in Pan et al. (2013)). Blue and yellow two types of lineations are seen only blue ones are considered in this work.

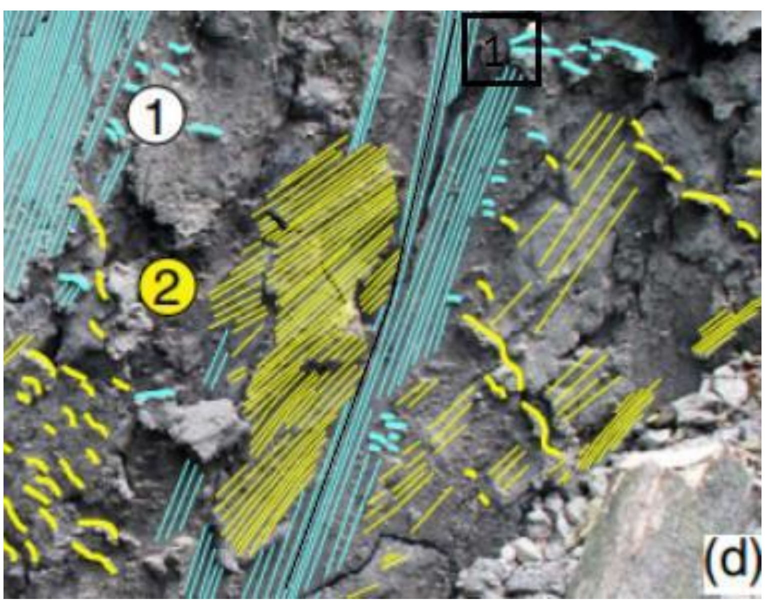

Fig. 14b. Traces of lineations black curve (traced by me).

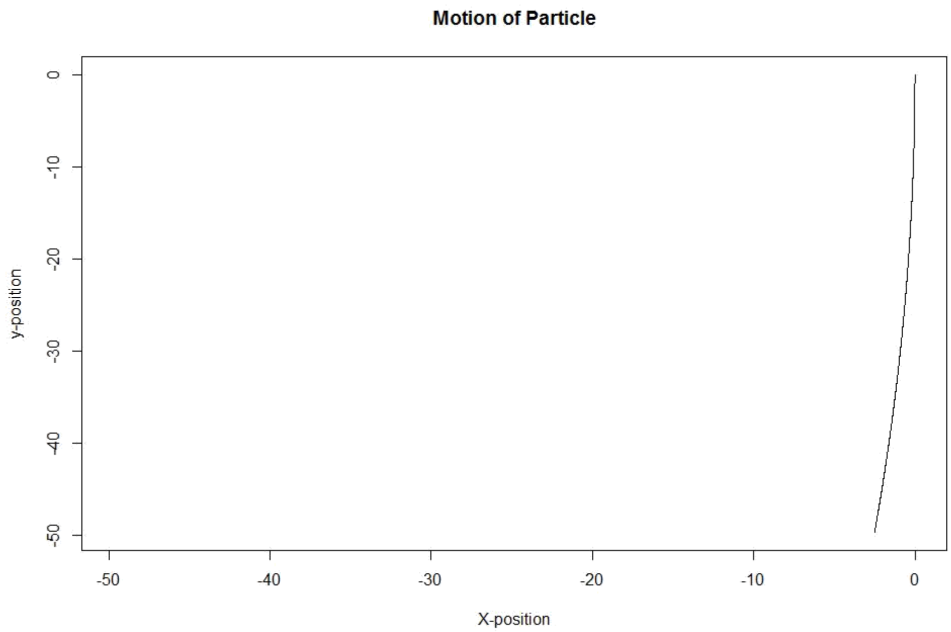

Fig. 14c. The modeled lineation for specific magnitudes of “ω/v” ratio, obtained by using The RStudio (Version1.0.153-2009-20017).

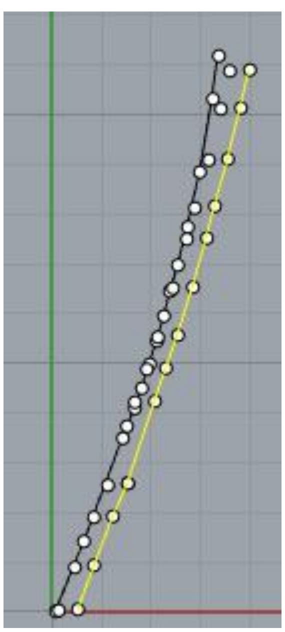

Fig. 14d. Fit between curves in the sub-figure b and the sub-figure c, black curve is natural lineation, and yellow curve is a model curve.

Fig. 15a. Natural lineations on fault planes (from fig. 11c in Pan et al. (2013)).

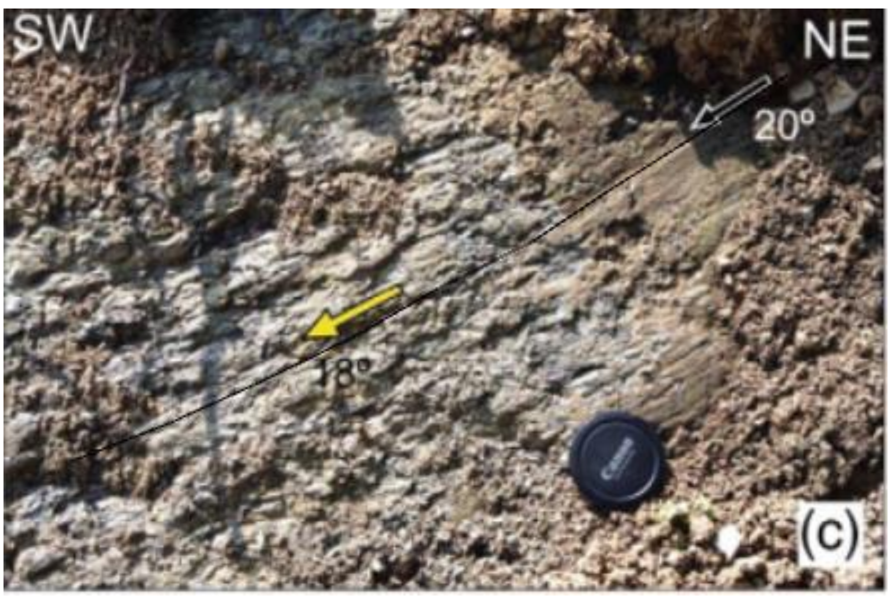

Fig. 15b. Traces of lineations black curve.

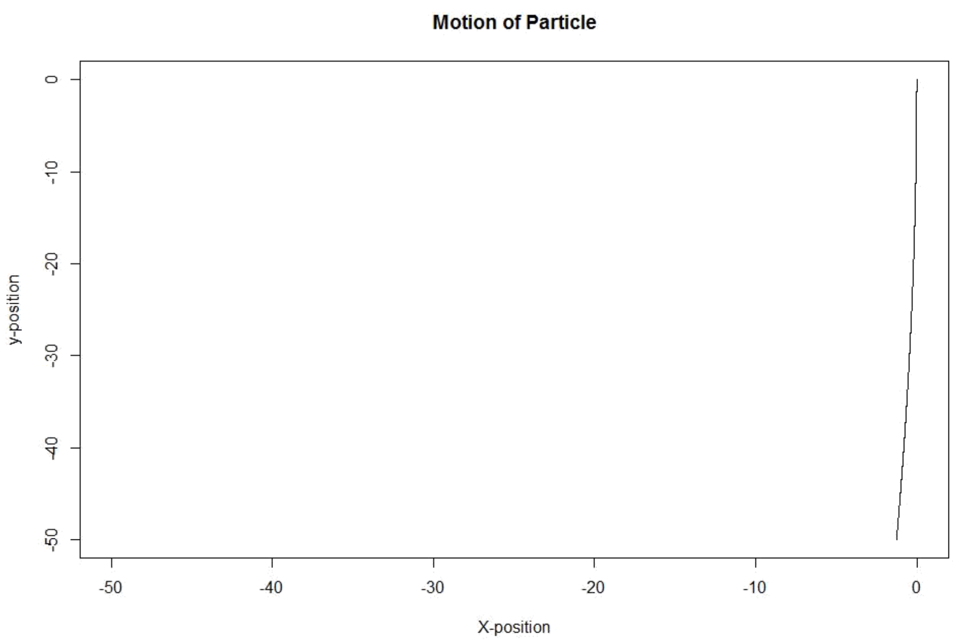

Fig. 15c. The modeled lineation for specific magnitudes of “ω/v” ratio, obtained by using The RStudio (Version1.0.153-2009-20017).

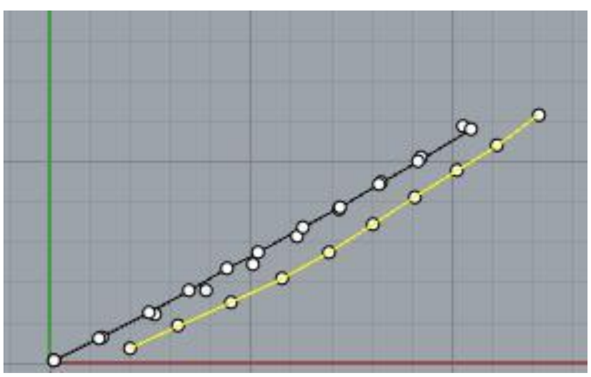

Fig. 15d. Fit between curves in the sub-figure b and the sub-figure c, black curve is natural lineation, and yellow curve is a model curve.

Fig. 16a. Natural lineations on fault planes (from fig. 2.4.a in Perrot (2013)).

Fig. 16b. Traces of lineations black curve.

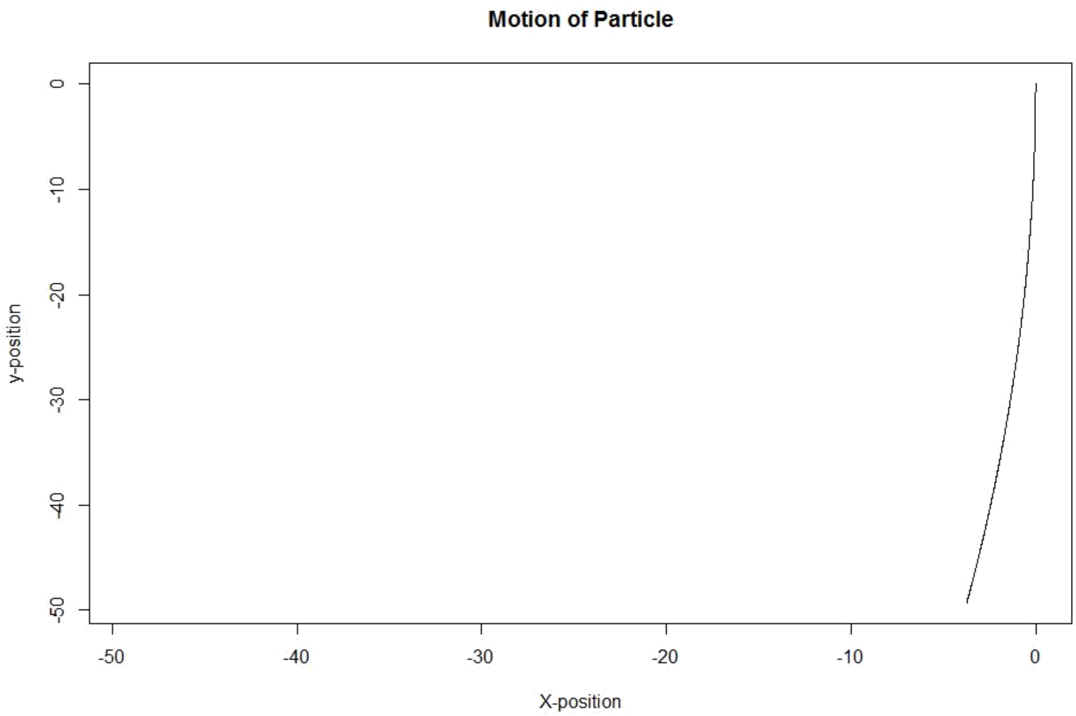

Fig. 16c. The modeled lineation for specific magnitudes of “ω/v” ratio, obtained by using The RStudio (Version1.0.153-2009-20017).

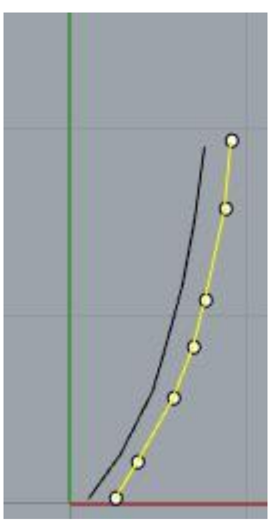

Fig. 16d. Fit between curves in the sub-figure b and the sub-figure c, black curve is natural lineation, and yellow curve is a model curve.

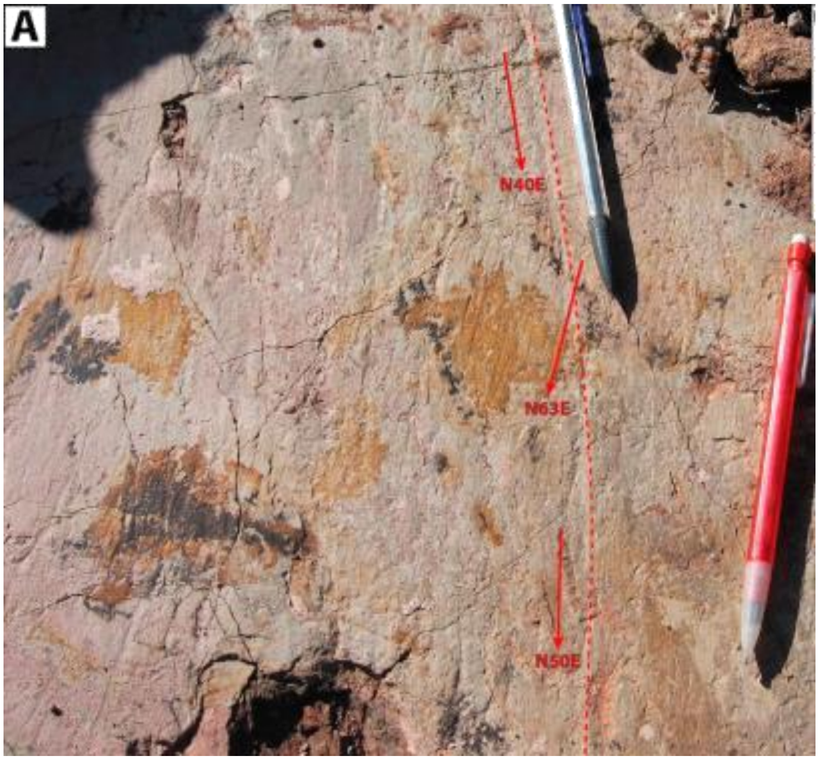

Fig. 17a. Natural lineations on fault planes (from fig. 4a in Singleton (2015)).

Fig. 17b. Traces of lineations black curve.

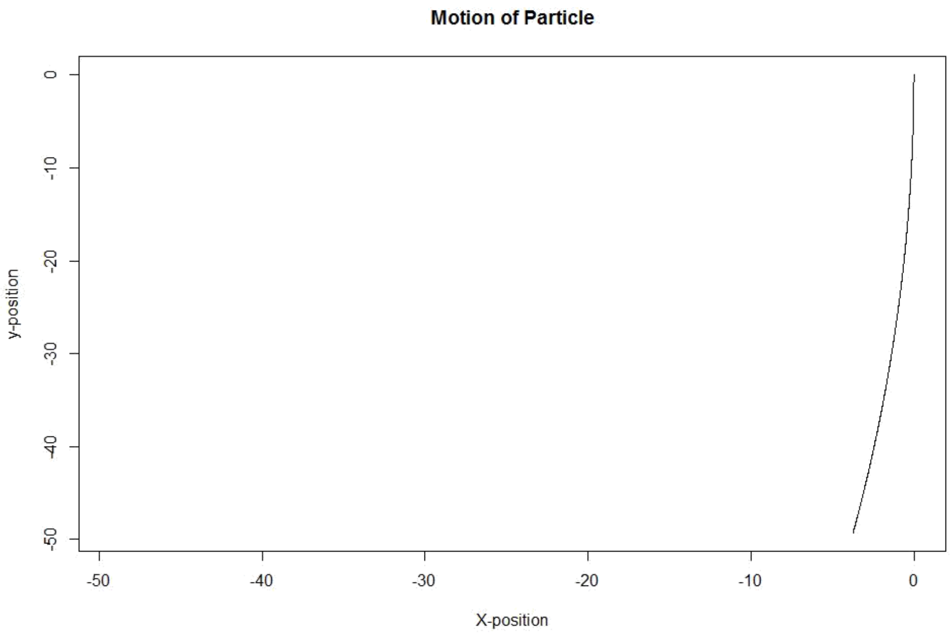

Fig. 17c. The modeled lineation for specific magnitudes of “ω/v” ratio, obtained by using The RStudio (Version1.0.153-2009-20017).

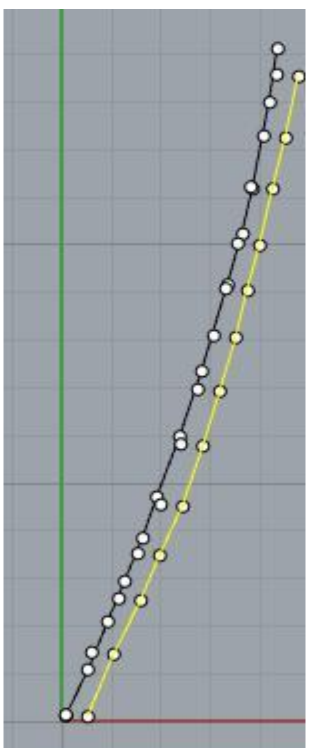

Fig. 17d. Fit between curves in the sub-figure b and the sub-figure c, black curve is natural lineation, and yellow curve is a model curve.

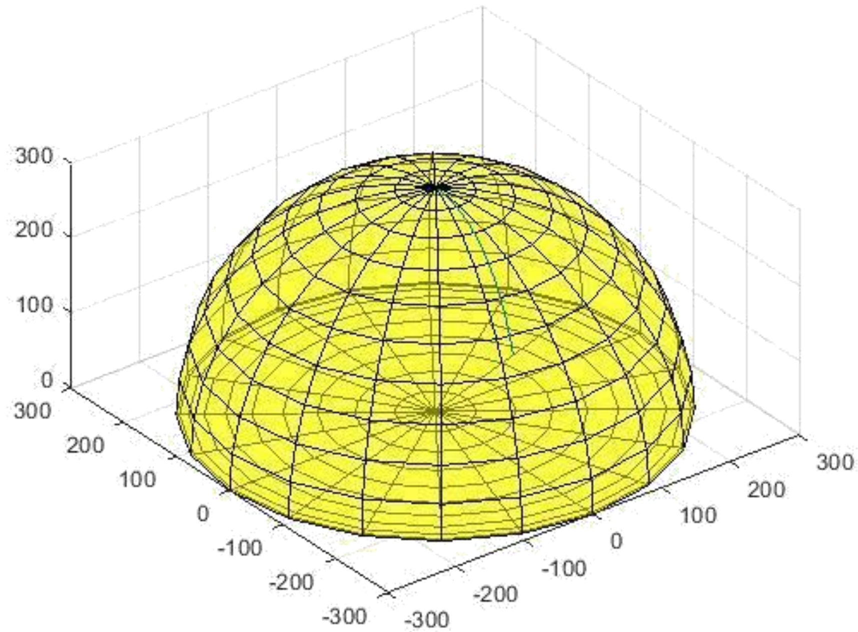

Fig. 18. The lineation pattern on a spherical surface for $\omega/v=0.6$, for (fig. 12 in Liu-Zang (2012)).

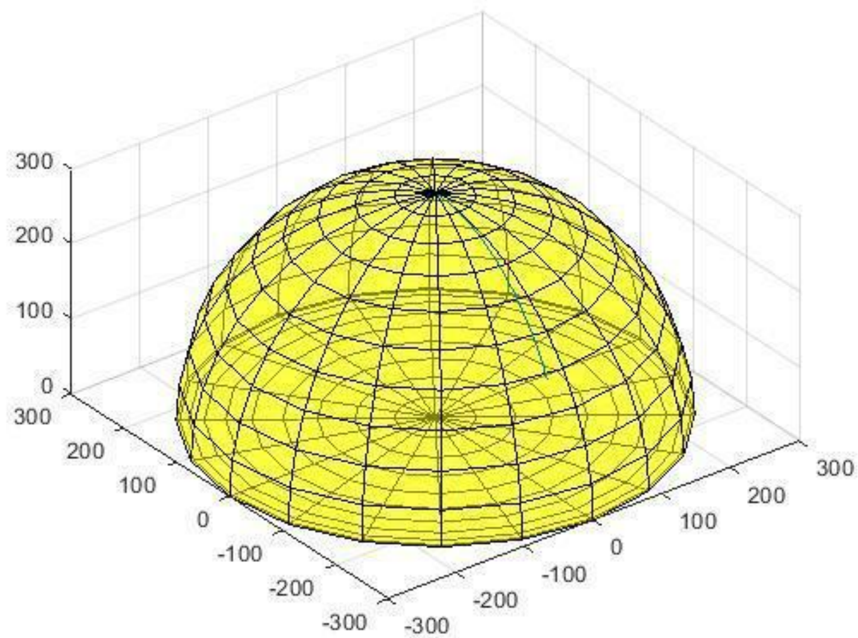

Fig. 19. The lineation pattern on a spherical surface for $\omega/v=2.4$, for (fig. 6b from Otsuki et al. (1997))

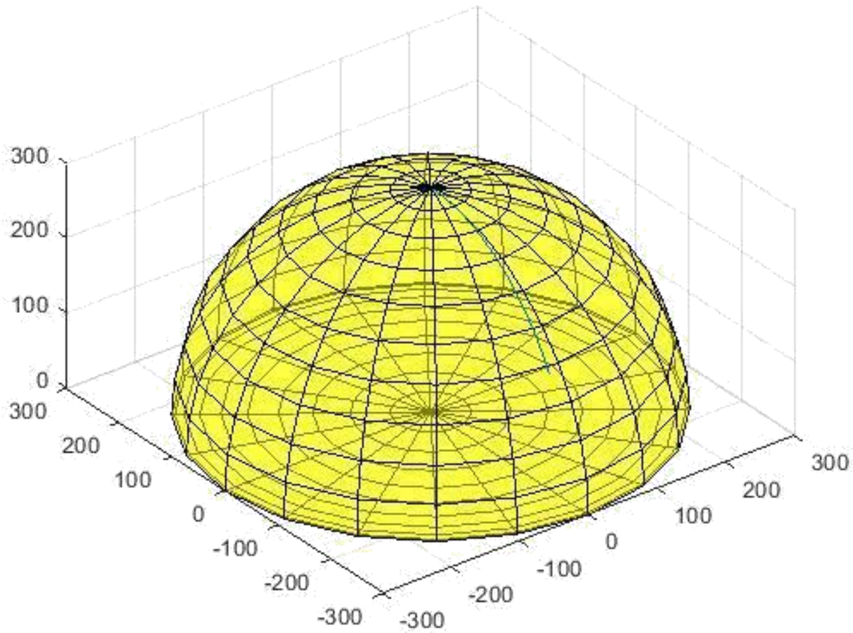

Fig. 20. The lineation pattern on a spherical surface for $\omega/v = 1.4$, for (fig. 6a in Otsuki et al. (1997))

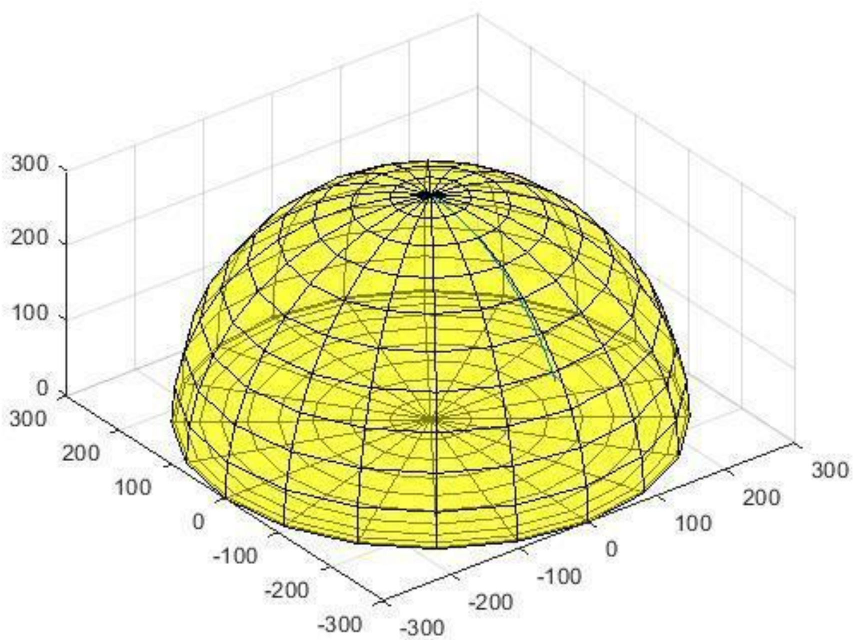

Fig. 21. The lineation pattern on a spherical surface for $\omega/v = 0.6$, for (fig. 7c in Pan et al. (2013))

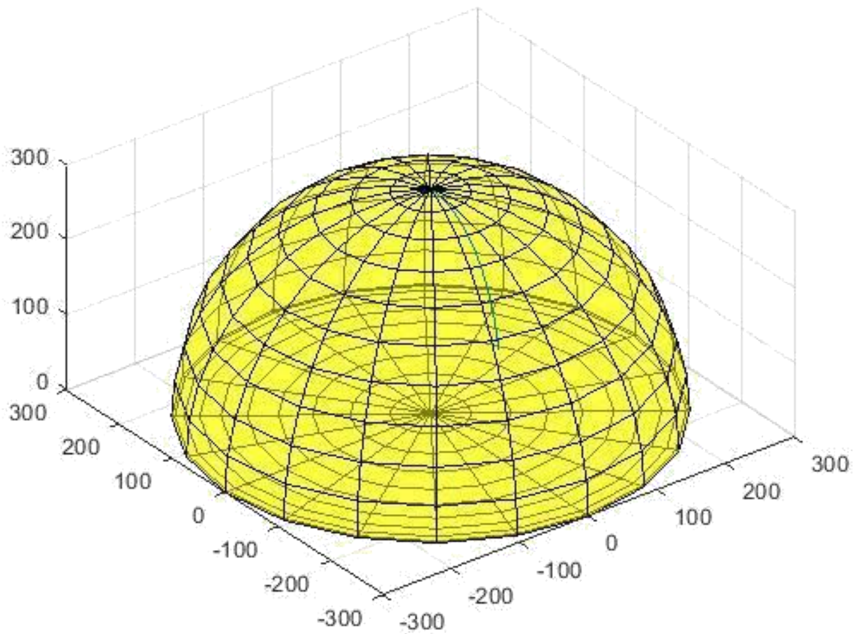

Fig. 22. The lineation pattern on a spherical surface for 0.4, this lineation pattern is for (fig. 4a in Xu et al. (2013))

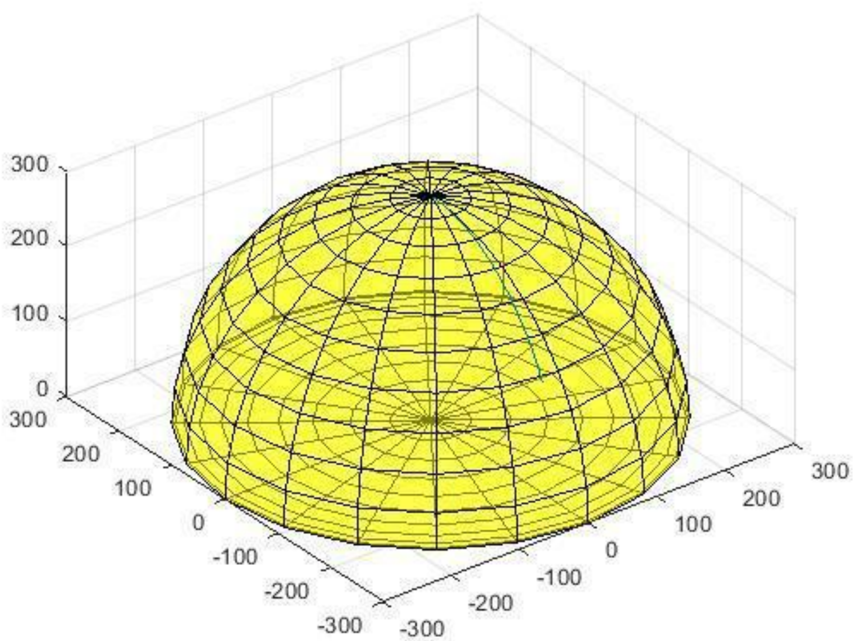

Fig. 23. The lineation pattern on a spherical surface for 0.2, for (fig. 4c in Xu et al. (2013))

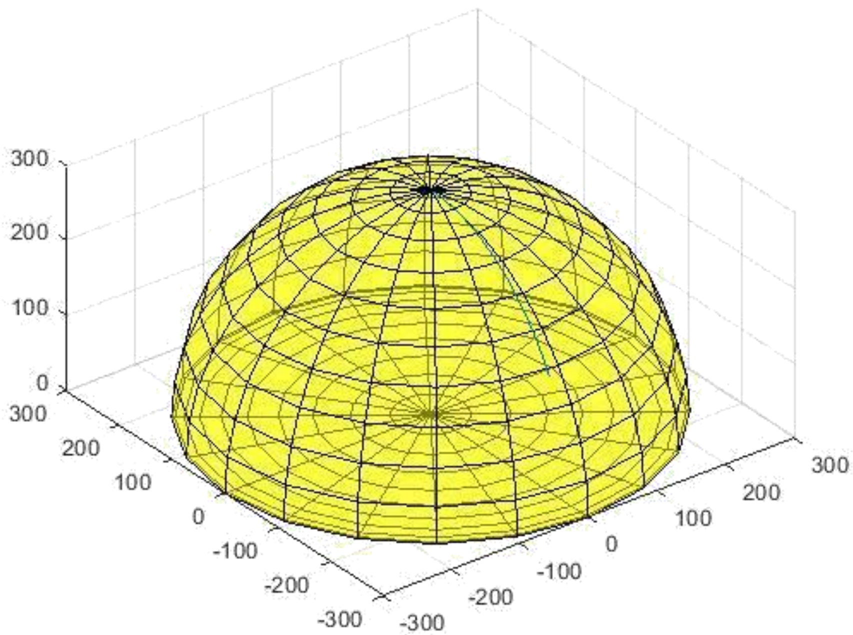

Fig. 24. The lineation pattern on a spherical surface for $\omega/v = 1.6$, for (fig. 2.4a in Perrot (2013))

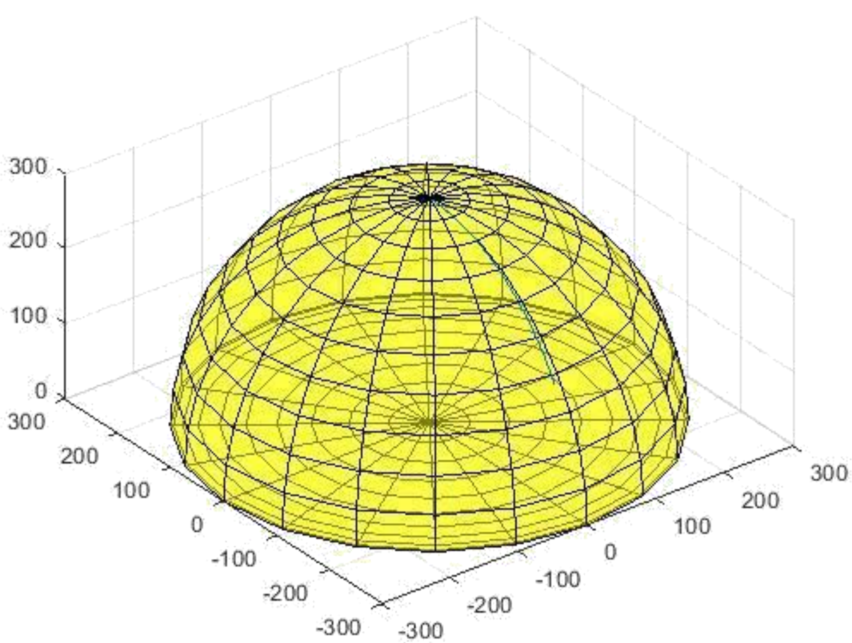

Fig. 25. The lineation pattern on a spherical surface for $\omega/v = 0.4$, for (fig. 8d in Xu et al. (2013))

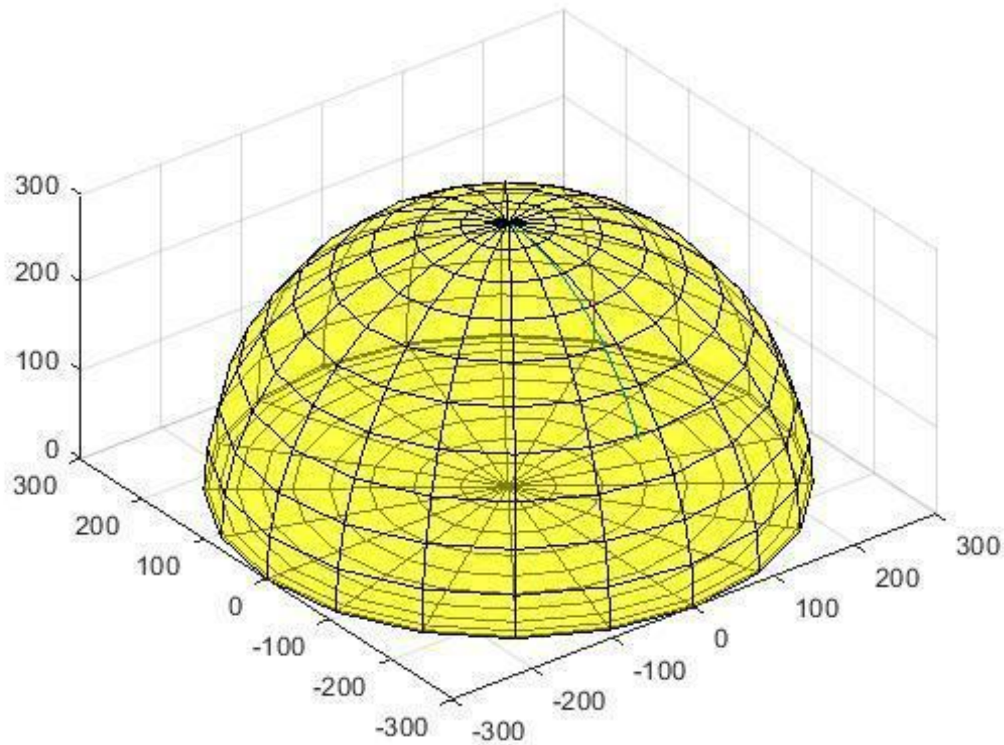

Fig. 26. The lineation pattern on a spherical surface for $\omega/v=0.2$, for (fig. 11c in Pan et al. (2013))

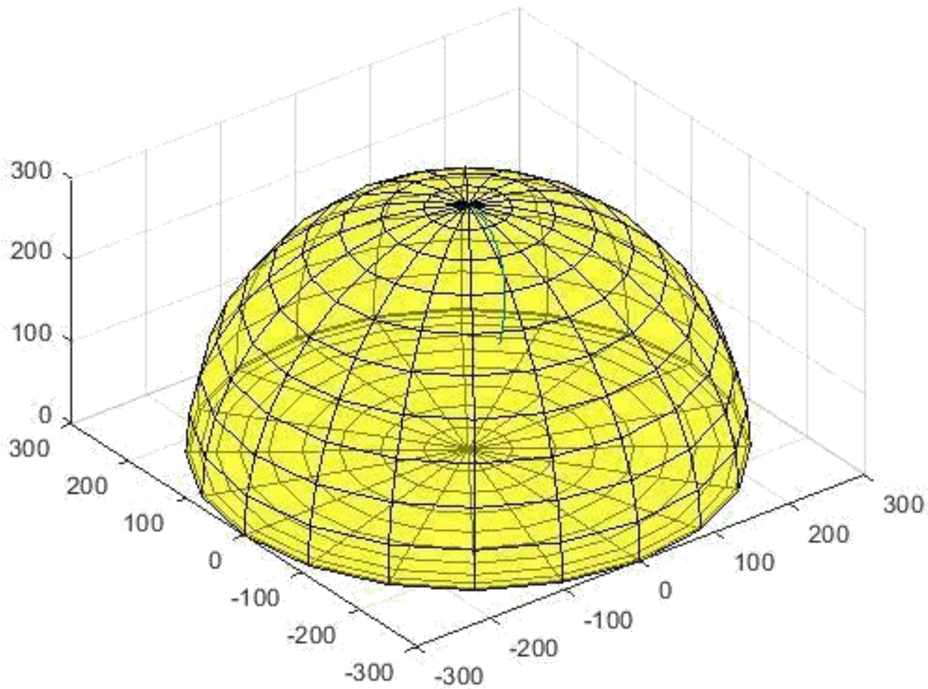

Fig. 27. The lineation pattern on a spherical surface for $\omega/v = 0.6$, for (fig. 8d in Singleton. (2015))

Discussions and Conclusions

Lineation pattern are simulated on planar and curviplanar fault planes for different ratios of rates of rotation and translation (ω/v) of the faulted blocks. With the simple computer codes presented in this work, one can now obtain such ratios from field photographs of fault planes containing slickensides and find out their tectonic implications. Analysis of the previously published images reveals the ω/v variation from 0.2 (San Miguelito range, Central México) to 2.4 (Hyogoken-Nambu, Japan). Roto-translational faults being an important component of many hydrocarbon reserves, this work can have a far-reaching implication in hydrocarbon geosciences. Different kinds of linear marks can develop on fault planes (review in Resor and Meer 2009). Such marks picked up in seismic images, known as corrugations, may not indicate slip direction of the fault (Ferrill et al. 1999). Therefore, those marks published by previous authors were avoided in analyzing in this study.

The second part of this work considers spherical geometry of the listric fault plane. Modeling listric fault surface in terms of a well-known curve or surface is commonplace in structural geological/ seismicity related analyses (e.g., Archuleta and Brune 1975). For example, Schultz (1987, 2002) numerically model the genesis of the listric strike-slip faults by considering circular arc-shaped curved fault planes for simplistic analyses and relate curvature of fault planes and their slip amounts. Schultz (1992) describes the mechanics of listric faults in 2D. For the sake of simplicity, his model considers the fault plane to be a circular arc. Mukherjee and Agarwal (2018) consider a circular fault plane in their 2D model of listric fault-induced shear heating. Ellis and McClay (1988) and Lohr et al. (2008) also presume the cylindrical geometry of the fault plane while modeling listric fault kinematics. However, rarely a parabolic fault plane is also considered in seismicity-related modeling (Griffin and Davies, web reference). A parabolic/paraboloid slip surface sounds mechanically feasible since such geometry of the slip surface has been deduced from Mohr-Coulomb failure criteria in slop-stability studies (e.g., Wriggers et al. 1990). If the fault plane in 3D is not perfectly spherical and the 3D coordinates of its surface are known then such set of coordinates can be input in the Matlab program.

Subsequently the lineations pattern for the different magnitudes of “ω/v” can also be obtained.

The natural faulting process can be more complicated than the “block models” shown in Billings(1954), which is followed in this work. At least seven issues are there. First, in block models, the faulted blocks are rigid. Therefore nature (magnitude and direction) of net slip is uniform along the fault trend. However, in reality, (i) a regional fault can change the slip pattern along its length, from thrust slip to oblique-slip (Gorum and Carranza 2015); and (ii) the fault slip is maximum usually at the middle portion of the fault length and decreases (uniformly) towards the two tips (Fossen 2016). These mean that the faulted blocks, in a regional-scale act as deformable solids. Second, Amos et al. (2007) report listric reverse faults from the Mackenzie Basin, New Zealand. When listric faults form a network (Claypool et al. 2002), the kinematics is expected to be more complicated. Third, faults with rotation components in their slip have been cursorily referred to have the temporally shifting pivot of rotation (Billings, 1972). Fourth, Pueyo et al. (2002) deduce from paleomagnetic studies from the External Sierras (Southern Pyrenees) an acceleration in the rotation rate of faulted blocks, from 5.5 to 9 ° Ma^{-2}. Ten times temporal increase of rotation rate has also been reported by Mochales et al. (2012) that has been linked with the emplacement of a thrust sheet. Fifth, A few natural faults have been reported where the geometries of curved lineations on the fault planes vary (e.g., Fig. 14.a). This means that over the same fault plane, “ω/v” ratio can change. Sixth, the curvature of fault planes may vary temporally (McClay and Ellis 1987). Seventh, Landslides and glacial abrasion sometimes leave curved lineations on (curved) planes. This work does not deal with fault networks, shifting pivot, accelerated rotation of fault-blocks, different “ω/v” ratio at different portions of the faulted block, changing the curvature of fault planes, and landslide and glacier-related lineations.

Appendix

Appendix 1

The RStudio (Version 1.0.153-2009-20017) code:

```
radial_vel<- -0.05 #in m/unit_time

ang_vel<- -0.01 # in rad/unit_time### One can, in general, have these as functions of t

t <- 0

x <- c(0)

y <- c(0)
steps<-
1000
step_size
<- 0.01
for(i in
1:steps ){

t <- t + step_size

x<- c(x,x[i]- 0.5*radial_vel*cos(ang_vel*t-pi/2))
y<- c(y,y[i]-radial_vel*sin(ang_vel*t-pi/2))

}

plot(x,y,main="Motion of Particle",
xlab="X-position", ylab="y-position",
xlim=c(min(y),0), ylim=c(min(y),
max(y)), type="l")

z=sqrt (300^2 - x^2 - y^2)
```

Appendix 2

The general Matlab program to produce lineations on spherical surfaces:

```
[x,y,z] = sphere(20);
R = 300;
xEast = R * x;
yNorth = R * y;
zUp= R * z;
zUp(zUp< 0) = 0;
figure('Renderer','opengl')
surf(xEast, yNorth, zUp,'FaceColor','yellow','FaceAlpha',0.5)
axis equal
hold on
z_p=[]
y_p= [];
x= [];
plot3(x,y_p,z_p)
```

References

(1) Afifi, A.S., Moustafa, A.R., Helmy, H.M. 2016. Fault block rotation and footwall erosion in the southern Suez rift: Implications for hydrocarbon exploration. Marine Petrol. Geol. 76, 377-396.

(2) Amos, C.B., Burbank, D.W., Nobes, D.C., Read, S.A.L. 2007. Geomorphic constraints on listric thrust faulting: Implications for active deformation in the Mackenzie Basin, South Island, NewZealand. J. Geophys. Res. 112, B03S11.

(3) Archuleta, R.J., Brune, J.N., 1975. Surface strong motion associated with a stick-slip event in a foam rubber model of earthquakes. Bull. Seismol. Soc. Am. 65, 1059-1071.

(4) Avagyan, A., Ritz, J.-F., Karakhanian, A., Philip, H., 2003. Dual near-surface rupturing mechanism during the 1988 Spitak earthquake (Armenia). Izvestia of the National Academy of Sciences of the Republic of Armenia LVI, 14 – 19.

(5) Bergh, S.G., Snoke, A.W., 1992. PolyphaseLaramide Deformation in the Shirley Mountains, South-Central Wyoming Foreland. Mountain Geol. 29, 85-100.

(6) Billings, M.P., 1954, Structural Geology. Second Edition. New York, Prentice-Hall,514 p

(7) Billings, M.P., 1972. Structural Geology, third ed. Prentice-Hall of India Pvt. Ltd, p. 178.

(8) Claypool, A.L., Klepeis, K.A., Dockrill, B., Clarke, G.L., Zwingmann, H., Tulloch, A. 2002. Structure and kinematics of oblique continental convergence in northern Fiordland, NewZealand. Tectonophys. 359, 329–358.

(9) Dasgupta, S., Mukherjee, S.. 2017. Brittle shear tectonics in a narrow continental rift: asymmetric non-volcanic Barmer basin (Rajasthan, India). J. Geol. 125, 561-591.

(10) Davis, T., Healy, D., Rivalta, E. 2019. Slip on wavy frictional faults: Is the 3rd dimension a sticking point? J. Struct. Geol. 119, 33-49.

(11) Dey, S., 2015. Geological history of the Kaladgi-Badami and Bhima basins, south India: sedimentarion in a Proterozoic intracratonic setup. In: Mazumder R, Eriksson PG (Eds) Precambrian Basins of India: Stratigraphic and Tectonic Context. Geol. Soc., London, Mem. 43, 283-296

(12) Dezes, P.J., Vannay, J.C., Steck, A., Bussy, F., Cosca, M., 1999. Synorogenic extension: quantitative constraints on the age and displacement of the zanskar shear zone. Geol. Soc. Am. Bull. 111, 364-374.

(13) Doblas, M. 1998. Slickenside kinematics indicators. Tectonophys. 295, 187-197.

(14) Doblas, M., 1997. Slickenside and fault surface kinematic indicators on active normal faults of the Alpine Betic cordilleras, Granada, southern Spain. J. Struct. Geol. 19, 159-170.

(15) Dorsey, R.J., Umhoefer, P.J., Renne, P.R., 1995. Rapid subsidence and stacked Gilbert-type fan deltas, Pliocene Loreto basin, Baja California Sur, Mexico. Sedi. Geol. 98, 181-204.

(16) Edwards, J.H., Kluesner, J.W., Silver, E.I., Brodsky, E.E., Brothers, D.S., Bangs, N.L., Kirpatrick, J.D., Wood, R., Okomoto, K., 2018. Corrugated megathrust revealed offshore from Costa Rica. Nature Geosci. 11, 197-203.

(17) Ellis, P.G., McClay, K.R. 1988. Listric extensional fault systems – results from analogue model of experiments. Basin Res. 1, 55-70.

(18) Escartin, J. et al. 2017. Tectonic structure, evolution, and the nature of oceanic core complexes and their detachment fault zones (138200N and 138300N, Mid Atlantic Ridge).Geophys. Geochem. Geosys. 18, 1451-1482.

(19) Ferrill, D.A., Stamatakos, J.A., Sims, D. 1999. Normal fault corrugation: implications for growth and seismicity of active normal faults. J. Struct. Geol. 21, 1027-1038.

(20) Fossen, H., 2016. Structural Geology. Second Edition. Cambridge University Press.ISBN-13: 978-1107057647.

(21) Ghosh, S.K., 1993. Structural Geology: Fundamentals and Modern Developments. Pergamon Press, p. 429.

(22) Griffin, J., Davies, G. Internet reference. Earthquake sources of the Australian plate margin. Revised models for the 2018 national tsunami and earthquake hazard assessments. URL: https://data.gov.au/dataset/earthquake-sources-of-the-australian-plate-margin-revised-modelsfor-the-2018-national-tsunami- (Accessed on 04-Dec-2018)

(23) Hjelle, Ø., 2014. A Hamilton–Jacobi framework for modelinggeological folding and deformation. Ph.D. thesis. pp. 80-88.

(24) Horst, A.J., Karson, J.A., Varga, R.J., 2018. Large Rotations of Crustal Blocks in the Tjörnes Fracture Zone of Northern Iceland. Tectonics 37, 1607-1625.

(25) Jackson, J., McKenzie, D., 1999.A hectare of fresh striations on the Arkitsa Fault, central Greece. J. Struct. Geol. 21, 1-6.

(26) Jayko, A.S., Bursik, M., 2012. Active Transtensional Intracontinental Basins: M Walker Lane belt. In: Busby C, Azor A. (Eds) Tectonics of Sedimentary Basins: Recent Advances. WileyBlackwell. pp. 226-248.

(27) Keary, P., Klepeis, K.A., Vine, F.J., 2013. Global Tectonics. Third Edition. Wiley-Blackwell. ISBN: ISBN 978-1-4051-0777-8.

(28) Kohn, M.J., Wieland, M.S., Parkinson, C.D., Upreti, B.N., 2004. Miocene faulting at plate tectonic velocity in the Himalaya of central Nepal. Earth Planet. Sci. Lett. 228, 299-310.

(29) Kusky, T.M., Bradley, D.T., Haeussler, P., 1997. Progressive deformation of the Chugach accretionary complex, Alaska, during a paleogene ridge-trench encounter. J. Struct. Geol. 19, 139-157.

(30) Liu-Zeng, J., Wen, L., Sun, J., Zhang, Z., Hu, G., Xing, X., Zeng, L., Xu, Q., 2010. Surficial Slip and Rupture Geometry on the Beichuan Fault near Hongkou during the Mw 7.9 Wenchuan Earthquake, China. Bull. Seismol. Soc. Am. 100, 2615-2650.

(31) Lohr, T., Krawczyk, C.M., Oncken, O., Tanner, D.C.. 2008. Evolution of a fault surface from 3D attribute analysis and displacement measurements. J. Struct. Geol. 30, 690-700.

(32) Mackenzier, D.E., 1993. Geology of the Featherbed Cauldron Complex, North

1-Eruptive Rocks and Post-Volcanic Sediments. Australian Geological Survey Organization.

(33) McClay, K.R., Ellis, P.G., 1987. Generation of extensional fault systems developed in model experiments. Geology 15, 341-344.

(34) Mandal, N., Chakraborty, C., 1989. Fault motion and curved slickenlines: a theoretical analysis. J. Struct. Geol. 11, 497-501.

(35) Marshak, S., Mitra, G., 1988. Basic Methods of Structural Geology. Prentice Hall. May, S.R., Ehman, K.D., Gray, G.G., Crowell, J.C., 1993. A new angle on the tectonic evolution of the Ridge Basin, a “strike-slip” basin in Southern California: Geol. Soc. Am.

(36) Mochale, T., Casas, A.M., Pueyo, E.L., Barnolas, A., 2012. Rotational velocity for oblique structures (Boltaña anticline, Southern Pyrenees). J. Struct. Geol. 35, 2-16.

(37) Morley, C.K., 2017. Syn- kinematic sedimentation at a releasing splay in the northern Minwun Ranges, Sagaing Fault zone, Myanmar: significance for fault timing and displacement. Basin Res. 29, 684-700.

(38) Mukherjee, S., 2014. Atlas of Shear Zone Structures in Meso-scale. Springer Geology. Cham. pp. 1-124. ISBN 978-3-319-0088-6.

(39) Mukherjee, S., 2015. Atlas of Structural Geology. Elsevier. Amsterdam. ISBN: 978-0-12-420152-1

(40) Mukherjeem S,, Agarwal I., 2018. Shear hear heat model for gouge free dip-slip listric normal faults. Marine Petrol. Geol. 98, 397-400.

(41) Mukherjee, S., Khonsari, M.M. 2017. Brittle rotational faults and the associated shear heating. Marine Petrol. Geol. 88, 551-554.

(42) Mukherjee, S., 2018. Moment of inertia for rock blocks subject to bookshelf faulting with geologically plausible density distributions. J. Earth Sys. Sci. 127, 80.

(43) Mukherjee, S., Khonsari, M.M., 2018. Inter-book normal fault-related shear heating in brittle bookshelf faults. . Marine Petrol. Geol. 97, 45-48.

(44) Nabavi, S.T., Alavi, S.A., Mohammadi, S., Ghassemi, M.R., Frehner, M., 2017. Analysis of transpression within contractional fault steps using finite-element method. J. Struct. Geol. 96, 1-20.

(45) Nevin, C.M., 1949. Principles of Structural Geology. John Wiley & Sons, New York. p. 88.

(46) Oohashi , K, Tamura T, 2016. An outcrop of the active Futagawa Fault, which ruptured during the 2016 Kumamoto earthquake. J. Geol. Soc. Japan 122, V-VI.

(47) Otsubo, M., Shigematsu, N., Imanishi, K., Ando, R., Takahashi, M., Azuma, T., 2013. Towards slip change based on curved slickenlines on fault scarps along Itozawa fault caused by 2011 Iwaki earthquake, northeast Japan. Tectonophysics 608, 970-979.

(48) Otsuki, K., Minagawa, J., Aono, M., Ohtake, M., 1997. On the Curved Striations of Nojima Seismic Fault Engraved at the 1995 Hyogoken-Nambu Earthquake, Japan. J. Seismol. Soc. Japan 49, 451-460.

(49) Pan, J., Li, H., Si, J., Pei, J., Fu, X., Chevalier, M.-L., Liu, D., 2014. Rupture process of the Wenchuan earthquake (Mw 7.9) from surface ruptures and fault striations characteristics.
Tectonophys. 619-620, 13-28.

(50) Pelz, K., Rohrmoser, I., Seyfried, H., 2006. Trishear fault propagation folding and faulting of growth strata in an extensional setting: Clues to the geometry of a listric oblique-slip fault. EGU06-A-08617; TS1.6-1TU1P-0878. (Abstract)

(51) Perrot, M., 2013. Étude Structuraleet Microstructurale de la Faille St-Josephetde la lignebaie Vertebromptondans les Appalaches du suddu Québec. University of Quebec in Montreal. Master of Earth Science Thesis. pp. 30.

(52) Price, S.P., Scott, B., 1994. Fault block rotations at the edge of a zone of continental extension; southwest Turkey. J. Struct. Geol. 16, 381-392.

(53) Pueyo, E.L., Millan, H., Pocovi, A.. 2002. Rotation velocity of a thrust: a paleomagnetic study in the External Sierras (Southern Pyrenees). Sedi. Geol. 146, 191-208.

(54) Resor, P.G., Meer, V.E., 2009. Slip heterogeneity on a corrugated fault. Earth Planet. Sci. Lett. 288, 483-491.

(55) Rodgers, D.A., Chinnery, M.A., 1969. The displacements and strains associated with a curved strike-slip fault. Eos, Trans., Am. Geophys. Union 50, 238.

(56) Rodriguez-Pinto, A., Pueyo, E.L., Calvin, P., Sanchez, E., Ramajo, J., Casas, A.M., Ramon, M.J., Pocovi, A., Barnolas, A., Roman, T., 2016. Rotational kinematics of a curved fold: The Balzes anticline (Southern Pyrenees). Tectonophys. 677–678, 171–189.

(57) Rowland, J.V., Sibson, R.H., 2001. Extensional fault kinematics within the Taupo Volcanic Zone, New Zealand: Soft- linked segmentation of a continental rift system. New Zealand J.Geol. Geophys. 44, 271-283.

(58) Rust, D., 1998. Contractional and extensional structures in the transpressive 'Big Bend' of the San Andreas fault, southern California. In: Holdsworth, R. E., Strachan, R.

A. & Dewey, J. E (Eds) 1998. Continental Transpressional and Transtensional Tectonics. Geol. Soc., London, Spec. Publ., 135, 119-126.

(59) Sanchez, VI., 2007. Structural evolution of the Neogene Gar basin, western Tibet: Implications for development and drainage patterns. MS thesis. University of Houston. pp. 47.

(60) Schultz, R.A. 1992. Mechanics of curved slip surfaces in rock. Engineering Analysis with Boundary Elements 10, 147-154.

(61) Schultz, R.A. 1987. Mechanics of curved strike-slip faults. Ph.D. thesis. Purdue University. p. 1-142.

(62) Seeber, L., Armbruster, J.G., 1995. The San Andreas Fault system through the Transverse Ranges as illuminated by earthquakes. J. Geophys. Res. 100, 8285-8310.

(63) Singleton, J.S., 2015.The transition from large-magnitude extension to distributed dextral faulting in the Buckskin-Rawhide metamorphic core complex, west-central Arizona. Tectonics 34, 1685-1708.

(64) Sporli, K.B., Rowland, J.V., 2007. Superposed deformation in turbidites and syn-sedimentary slides of the tectonically active Miocene Waitemata Basin, northern New Zealand. Basin Res. 19, 199–216.

(65) Taiwan Petroleum Exploration Division, Chinese Petroleum Corporation, 1992. Petroleum Geology of Taiwan, Issues 27-29.

(66) Tapsoba, B., Howard, W., 2017. Modeling the geometry of Shear Zone hosted gold + bismuth telluride bearing quartz veins at the historic Bunker Hill mine, south of Nelson, B.C.- a covert , mildly, folded Tension vein array. Orogeny to Ore: Cordilleran Tectonics Workshops. University of British Coloumbia. pp. 88-90.

(67) Tearpock, D.J., Bischke, R.E., 2002. Applied Sub-surface Geological Mapping With Structural Methods. Second Edition. Prentice Hall, New Jersey. ISBN 0-13-859315-9.

(68) Torabi A, Alaei B, Libak A. 2019. Normal fault 3D geometry and displacement revisited: Insights from faults in the Norwegian Barents Sea. Marine Petrol. Geol. 99, 135-155.

(69) Twiss, R.. Portzman, G.M., Hurst, S.D., 1991.Theory of slickenline patterns based on the velocioty gradient tensor and microrotation. Tectonophys. 186, 215-239.

(70) Twiss, R.J., Gefell, M.J., 1990., Curved slickenfibers: a new brittle shear sense indicator with application to a sheared serpentinite. J. Struct. Geol. 12, 471-481.

(71) URL: https://www.researchgate.net/profile/Jonathan_Griffin5/publication/328518053_Earthquake_sou rces_of_the_Australian_plate_margin_Revised_models_for_the_2018_national_tsunami_and_earthquake_hazard_assessments/links/5bd23715299bf1124fa36bab/Earthquake-sources-of-theAustralian-plate-margin-Revised-models-for-the-2018-national-tsunami-and-earthquake-hazardassessments.pdf (Accessed on 24-Nov-2018)

(72) Vauchez, A., 1987. Brevard fault zone, southern Appalachians: A medium-angle, dextral, Alleghanian shear zone. Geology 15, 669-672.

(73) Wriggers, P., Vu Van, T., Stein, E., 1990. Finite element formulation of large deformation impact-contact problems with friction. Comp. Struct. 37, 319-331.

(74) Xu, S., Nieto-Samaniego, A.F., Alaniz-Alvarez, S.A., 2013. Origin of superimposed and curved slickenlines in San Miguelito range, Central México. Geol. Acta 11, 103-112.

(75) Zhang, P.-Z., Wen, X.-z., Shen, Z.-K., Chen, J.-h., 2010. Oblique, High-Angle, Listric-Reverse Faulting and Associated Development of Strain: The Wenchuan Earthquake of May 12, 2008, Sichuan, China. Ann. Rev. Earth Planet. Sci. 38, 351-380.